

**Replacement of the ISIS horizontal  
injection beamline  
TRI-DN-22-05**

**Document Type: Design Note**

**Release: 02**

**Release Date: 2022-10-25**

**Authors: M. Marchetto, S. Saminathan**

	<b>Name:</b>	<b>Signature:</b>
<b>Authors:</b>	<b>M. Marchetto</b>	<b>REVIEW RECORD</b>
	<b>S. Saminathan</b>	
<b>Reviewed By:</b>	<b>R. Baartman</b>	
	<b>Y.N. Rao</b>	
	<b>V. Verzilov</b>	
<b>Approved By:</b>	<b>Y. Bylinskii</b>	

*Note: Before using a copy (electronic or printed) of this document you must ensure that your copy is identical to the released document, which is stored on TRIUMF's document server.*

Replacement of the ISIS horizontal injection beamline TRI-DN-22-05		
Document-218327	Release No. 02	Release Date: 2022-10-25

### History of Changes

Release number	Date	Description of changes	Authors
1	<a href="#">Link to version history</a>		
02	2022-10-25	The total length of the matching section is increased by 76.2 mm according to the required spacing in I2. Updates on the matching and vertical bend sections. Optics modules for the 5:1 selector and buncher optics have been included.	M. Marchetto S. Saminathan

**Keywords:** P481, ISIS, cyclotron, injection, electrostatic, beamline, I1, I2

**Distribution List:** Author, Reviewers, Approver, M. Brownell, P. Dirksen, T. Hruskovec, K. Jayamanna, E. Klassen, O. Law, T. Planche, D. Portilla, D. Preddy, D. Rowbotham, T. Stanford, T. Sytchougova, T. Tateyama, D. Yosi-fov, V. Zvyagintsev.

# 1 Introduction

The Ion Source and Injection System (ISIS) beamline is used to transport the 300 keV H<sup>-</sup> beam from the ion source to the injection of TRIUMF 500 MeV cyclotron. The vertical section of the beamline was upgraded in 2011 [1, 2]; since then the operation of this section is very robust and reliable, whereas the horizontal section of the beamline is very demanding in maintenance, and it presents a high risk of downtime due to aging equipment (optics, diagnostic, vacuum, etc.).

The horizontal beam line, which layout is represented in figure 1, is going to be re-designed with well proven optical concepts, and modern technologies already used in the vertical section, and more recently in the ARIEL RIB transport system [3]; this is expected to produce a more efficient system, easier to maintain and tune. Such technologies include metal seals (ConFlat® flanges), and ultra-high vacuum (UHV) materials and assembly procedures in order to reach a lower pressure (10<sup>-8</sup> Torr), with respect to the present installation, and hence reduce beam losses due to residual gas interaction.

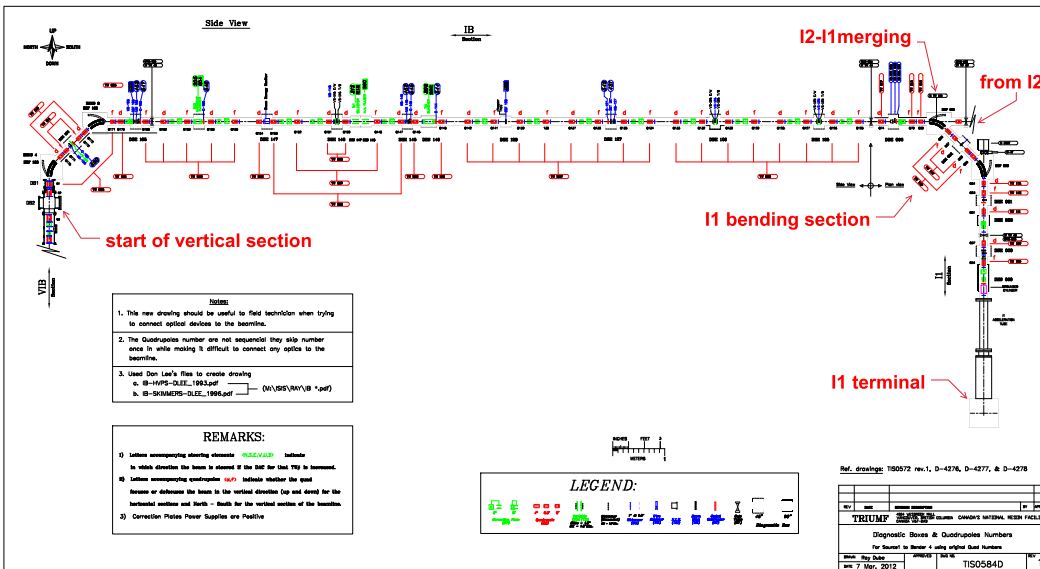


Figure 1: Schematic of the ISIS horizontal injection line from I1 terminal (bottom right) to the vertical beamline (top left). The I2 section merges into the I1 horizontal bend (top right) along the South-North direction.

Replacement of the ISIS horizontal injection beamline TRI-DN-22-05		
Document-218327	Release No. 02	Release Date: 2022-10-25

The injection beamline consists of electrostatic optics modules such as matching sections, periodic sections, the 90 degree achromatic bend sections. Elements of the injection line include also bunchers (multiple or multi-harmonics) and a high-energy pulser. Appropriate diagnostic equipment is required in order to ensure the beam is properly matched out of the ion source, through the transport system, and into the cyclotron.

The new injection beamline is planned to be controlled via EPICS like all the ISAC/ARIEL accelerator systems. The vacuum system of the present installation has already been migrated to EPICS. It is foreseen though that some cross talking with the original Central Control System (CCS) will still be necessary to exchange information and/or interlock signals from the cyclotron.

## 1.1 Purpose

This document presents the main features of the new ISIS injection horizontal beamline including the optics design, and the system to compensate the cyclotron stray field within the vacuum envelope.

## 1.2 Scope

The P481 project scope covers two beamline sections:

1. I1 terminal to start of the vertical injection beamline [1] (original scope)
2. I2 terminal to I1 injection beamline (extension)

The two sections merge at the I1 horizontal bend.

## 1.3 Related document

The following documents are respectively the input and one of the outputs (this design note being another one) of the design process as described in [TSOP-06](#):

- **Document-190702**: Requirements for the cyclotron injection beamline upgrade [4]
- **Document-218366**: Coordinates for the optical and diagnostics elements in the ISIS horizontal beamline upgrade

Replacement of the ISIS horizontal injection beamline TRI-DN-22-05		
Document-218327	Release No. 02	Release Date: 2022-10-25

## 2 Acronyms

The following table 1 defines the abbreviations used in the document

Acronym	Definition
BPM	Beam position monitor
BUNCH	Buncher
COL	Collimator
EQ	Electrostatic quadrupole
EB	Electrostatic bender
FC	Faraday cup
HED	High energy dump
HEP	High energy pulser
5T1S	5:1 Selector
IB	Horizontal injection beamline (main)
IB1	Horizontal injection beamline from I1 to IB
IB2	Horizontal injection beamline from I2 to IB
I1	Ion (source) injection terminal 1
I2	Ion (source) injection terminal 2
PM	Profile monitor
TNIM	Toroid non-intercepting monitor
VIB	Vertical injection beamline
XCB (XST) <sup>1</sup>	X correction bender
YCB (YST)	Y correction bender
XEMIT	X emittance scanner
XSLIT	X slit
YEMIT	Y emittance scanner
YSLIT	Y slit

Table 1: Definitions of the abbreviations used in the document.

Replacement of the ISIS horizontal injection beamline TRI-DN-22-05		
Document-218327	Release No. 02	Release Date: 2022–10–25

### 3 Ion beam transport

The new horizontal section of the injection beamline will be used to transport the extracted ion beams from the ion source injection terminals I1 and I2 through the vertical injection beamline. Basic beam transport requirements for the horizontal injection beamline are specified in table 2 and detailed specifications are provided in Ref. [4] & [5]. Optics design of the new ion source injection terminal I2 is described in Ref. [6]. In this design note, the optics design for transporting a 300 keV ion beam through the horizontal injection beamline has been presented. The horizontal injection beamline con-

Beam species	H <sup>-</sup>
Beam energy	300 keV
Maximum beam intensity	1 mA
Beam emittance at 300 keV	12.0 $\mu\text{m}$
Pulsed Frequency	375 Hz–1.126 kHz
Beam duty cycle	0.1% – 99.0%
Bunching frequency	23.06 MHz
Localized maximum beam loss	< 10 $\mu\text{A}$
Vacuum	$\leq 1 \times 10^{-7}$ torr

Table 2: Summary of basic beam transport requirements [4].

sists of electrostatic optics modules such as matching sections, a periodic section, the 90° achromatic bend section and low beta insertion. Specifications for these optics modules are provided in Sec. 4 and the specification for the optical elements used in the modules are given in Sec. 5. The optical elements and the required diagnostics devices are listed in the table 4, 6 & 7 along with their EPICS label in a sequential order.

The ion beam transport calculations have been performed for the given beamline layout at the I1 and I2 injection terminals. The position of the ion source at I1 and I2 as well as the horizontal injection beamline with respect to the vertical injection beamline of the cyclotron has been fixed. This gives

<sup>1</sup>-CB is used for EPICS label, -ST is used for figures.

Replacement of the ISIS horizontal injection beamline TRI-DN-22-05		
Document-218327	Release No. 02	Release Date: 2022-10-25

a constraint on the beamline layout and its total length. Figure 2 shows the calculated beam envelope through the horizontal injection beamline for transporting an extracted ion beam from the I2 terminal by using the code TRANSOPTR. The beam envelope calculations have been performed from the beam waist at the exit of 300 keV accelerating column and up to the common periodic section for the I2 and I1 beam transport. In these envelope calculations, the space-charge effect is taken into account for a 295 keV ion beam with a given beam intensity of about 1 mA.

Figure 3 shows the calculated beam envelope through the horizontal injection beamline up to the exit of the 90° vertical bend section for transporting the ion beams from the I1 terminal. The section of the beamline between the quadrupoles EQ24 and EQ25 consists of a 45° electrostatic bender for switching the beam transport between I2 and I1 terminals. This section of the beamline is called the merger section. This works as a periodic section for transporting the beam from the I2 terminal, whereas it works as a part of the 90° achromatic bend section while transporting the beam from the I1 terminal. The beamline downstream of the merger section, i.e., from EQ25 onwards, is a common beamline for transporting the ion beams from both I2 and I1 terminals. Here, the polarity of quadrupole EQ26 needs to change according to the selection of beam transport either from I1 or I2 terminal. The concept of the optical modules is similar to the optics modules in the existing beamline. However, the length of the optical module differs from the existing one. Also, we have added a new optical module called low beta insertion to accommodate the buncher at the location of, beam waist, in addition to the function of order-reversing. The required optical modules and their specifications are described in the following Sec. 4.

Replacement of the ISIS horizontal injection beamline TRI-DN-22-05		
Document-218327	Release No. 02	Release Date: 2022-10-25

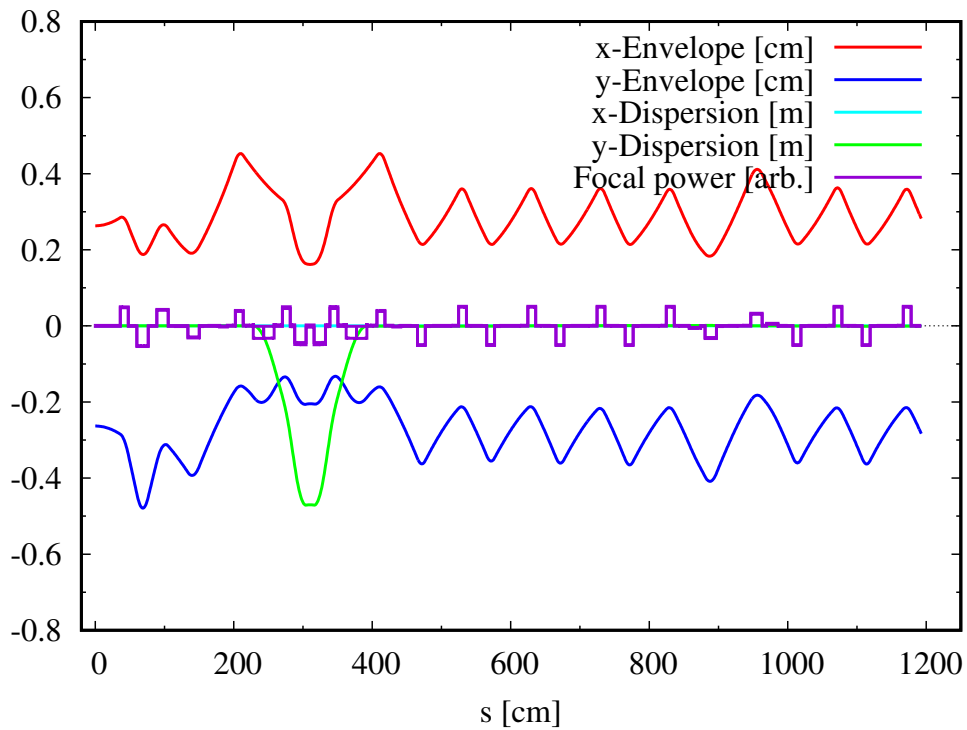


Figure 2: Calculated beam envelope (2RMS, positive for  $x$ , negative for  $y$ ) for an extracted beam of 1 mA 295 keV  $H^-$  beam from the I2 terminal through the section of horizontal injection beamline with  $\varepsilon_{4rms} = 6 \mu\text{m}$ .

Replacement of the ISIS horizontal injection beamline TRI-DN-22-05		
Document-218327	Release No. 02	Release Date: 2022-10-25

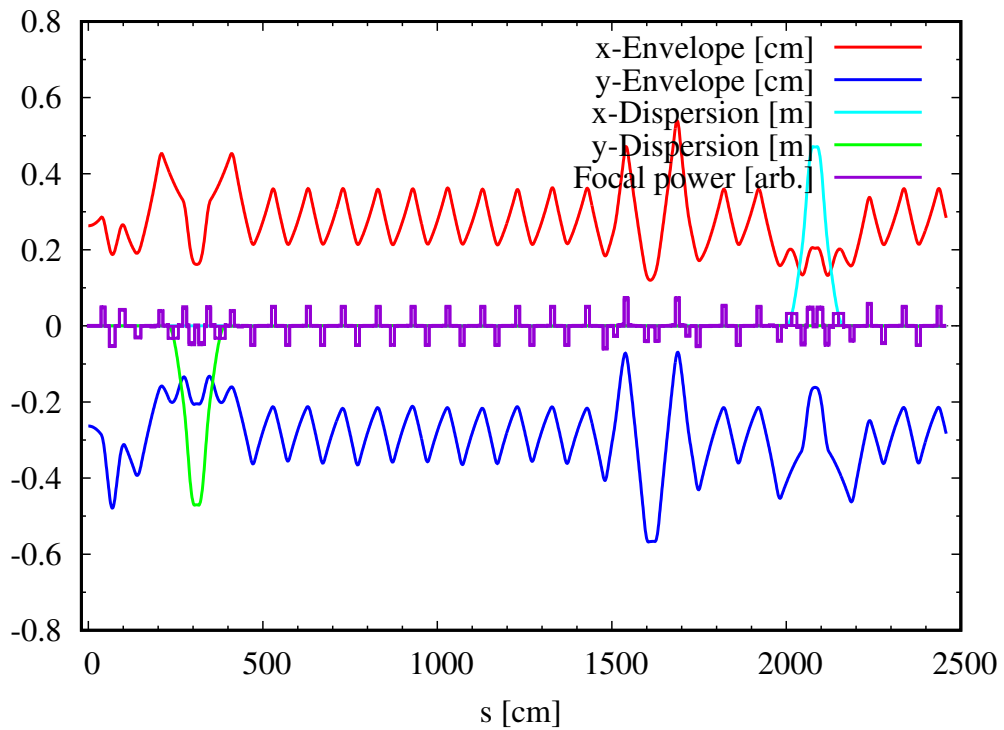


Figure 3: Calculated beam envelope (2RMS, positive for  $x$ , negative for  $y$ ) for an extracted beam of 1 mA 295 keV  $H^-$  beam from the I1 terminal through the section of horizontal injection beamline with  $\varepsilon_{4rms} = 6 \mu\text{m}$ .

Replacement of the ISIS horizontal injection beamline TRI-DN-22-05		
Document-218327	Release No. 02	Release Date: 2022-10-25

Elements	Function	EPICS lable	Elements	Function	EPICS lable
XST01C	–	IB2:XCB1C	EQ06	F-Quad	IB2:Q6
DUMP01C	–	IB2:DUMP1C	EB06	–	IB2:B6
FC01C	–	IB2:FC1C	EQ07	F-Quad	IB2:Q7
PM01C	–	IB2:PM1C	EQ08	D-Quad	IB2:Q8
YST01C	–	IB2:YCB1C	PM08	–	IIT2:PM8
COL01C	–	IB2:COL1C	EQ09	D-Quad	IB2:Q9
EQ01	F-Quad	IB2:Q1	EQ10	F-Quad	IB2:Q10
TNIM01	–	IB2:TNIM1	EB10	–	IB:B1
EQ02	D-Quad	IB2:Q2	EQ11	F-Quad	IB:Q1
EQ03	F-Quad	IB2:Q3	EQ12	D-Quad	IB:Q2
EQ04	D-Quad	IB2:Q4	YST12	–	IB:YCB2
YST04	–	IB2:YCB4	FC12	–	IB:FC2
SK04	–	IB2:SK4	TNIM12	–	IB:TNIM2
FC04	–	IB2:FC4	PM12	–	IB:PM2
PM04	–	IB2:PM4	XST12	–	IB:XCB2
XST04	–	IB2:XCB4	EQ13	D-Quad	IB:Q3
EQ05	D-Quad	IB2:Q5	EQ14	F-Quad	IB:Q4
			EQ15	D-Quad	IB:Q5

Table 3: List of optical and diagnostics elements in the horizontal injection beamline for transporting ion beams from the I2 terminal.

Replacement of the ISIS horizontal injection beamline TRI-DN-22-05		
Document-218327	Release No. 02	Release Date: 2022-10-25

Elements	Function	EPICS lable	Elements	Function	EPICS lable
EQ16	F-Quad	IB:Q6	YST20	–	IB:YCB10
YST16	–	IB:YCB6	XST20	–	IB:XCB10
FC16	–	IB:FC6	PM20	–	IB:PM10
SK16	–	IB:SK6	COL20	–	IB:COL10
PM16	–	IB:PM6	EQ21	D-Quad	IB:Q11
XST16	–	IB:XCB6	EQ22	F-Quad	IB:Q12
EQ17	D-Quad	IB:Q7	SK22	–	IB:SK12
EQ18	F-Quad	IB:Q8	YST22	–	IB:YCB12
EQ19	D-Quad	IB:Q9	FC22	–	IB:FC12
EQ20	F-Quad	IB:Q10	XST22	–	IB:XCB12
SK20	–	IB:SK10	EQ23	F/D-Quad	IB:Q13
			EQ24	D-Quad	IB:Q14

Table 4: List of optical and diagnostics elements in the horizontal injection beamline for transporting ion beams from the I2 terminal.

Elements	Function	EPICS lable	Elements	Function	EPICS lable
XST01C	–	IB1:XCB1C	EQ26	D-Quad	IB:Q16
DUMP01C	–	IB1:DUMP1C	YST26	–	IB:YCB16
FC01C	–	IB1:FC1C	COL26	–	IB:COL16
PM01C	–	IB1:PM1C	FC26	–	IB:FC16
YST01C	–	IB1:YCB1C	TNIM26	–	IB:TNIM16
COL01C	–	IB1:COL1C	SK26	–	IB:SK16
EQ01	F-Quad	IB1:Q1	PM26	–	IB:PM16
TNIM01	–	IB1:TNIM1	XST26	–	IB:XCB16
EQ02	D-Quad	IB1:Q2	EQ27	D-Quad	IB:Q17
EQ03	F-Quad	IB1:Q3	EQ28	F-Quad	IB:Q18
EQ04	D-Quad	IB1:Q4	XEMIT28	–	IB:XEMIT18
XST04	–	IB1:YCB4	YEMIT28	–	IB:YEMIT18
SK04	–	IB1:SK4	EQ29	D-Quad	IB:Q19
FC04	–	IB1:FC4	EQ30	F-Quad	IB:Q20
PM04	–	IB1:PM4	YST30	–	IB:YCB20
YST04	–	IB1:XCB4	FC30	–	IB:FC20
EQ05	D-Quad	IB1:Q5	SK30	–	IB:SK20
EQ06	F-Quad	IB1:Q6	PM30	–	IB:PM20
EB06	–	IB1:B6	XST30	–	IB:XCB20
EQ07	F-Quad	IB1:Q7	EQ31	D-Quad	IB:Q21
EQ08	D-Quad	IB1:Q8	EQ32	F-Quad	IB:Q22
SK08	–	IB1:SK8	EQ33	D-Quad	IB:Q23
PM08	–	IB1:PM8	EQ34	F-Quad	IB:Q24
EQ09	D-Quad	IB1:Q9	YSL34	–	IB:YSL24
EQ10	F-Quad	IB1:Q10	XSL34	–	IB:XSL24
EB14	–	IB:B14	PM34	–	IB:PM24
EQ25	F-Quad	IB:Q15			

Table 5: List of optical and diagnostics elements in the horizontal injection beamline for transporting ion beams from the I1 and I2 terminals.

Replacement of the ISIS horizontal injection beamline TRI-DN-22-05		
Document-218327	Release No. 02	Release Date: 2022-10-25

Elements	Function	EPICS lable	Elements	Function	EPICS lable
YST34	–	IB:YCB24	FC42	–	IB:FC32
XST34	–	IB:XCB24	TNIM42	–	IB:TNIM32
SK34	–	IB:SK24	PM42	–	IB:PM32
EQ35	D-Quad	IB:Q25	XST42	–	IB:XCB32
EQ36	D-Quad	IB:Q26	SK42	–	IB:SK32
EQ37	F-Quad	IB:Q27	EQ43	D-Quad	IB:Q33
EQ38	F-Quad	IB:Q28	EQ44	F-Quad	IB:Q34
YST38	–	IB:YCB28	EQ45	D-Quad	IB:Q35
XST38	–	IB:XCB28	EQ46	F-Quad	IB:Q36
YSL38	–	IB:YSL28	SK46	–	IB:SK36
XSL38	–	IB:XSL28	COL46	–	IB:COL36
PM38	–	IB:PM28	BUNCH46	–	IB:BUNCH36
SK38	–	IB:SK28	EQ47	D-Quad	IB:Q37
EQ39	D-Quad	IB:Q29	PM47	–	IB:PM37
EQ40	F-Quad	IB:Q30	EQ48	D-Quad	IB:Q38
EQ41	D-Quad	IB:Q31	EQ49	F-Quad	IB:Q39
EQ42	F-Quad	IB:Q32	HEP39	–	IB:HEP39
YST42	–	IB:YCB32	5:1SELECTOR	–	IB:5T1S39
COL42	–	IB:COL32			

Table 6: List of optical and diagnostics elements in the horizontal injection beamline for transporting ion beams from the I1 and I2 terminals.

Replacement of the ISIS horizontal injection beamline TRI-DN-22-05		
Document-218327	Release No. 02	Release Date: 2022-10-25

Elements	Function	EPICS lable	Elements	Function	EPICS lable
EQ50	D-Quad	IB:Q40	EQ58	F-Quad	IB:Q48
XSL50	–	IB:XSL40	EQ59	D-Quad	IB:Q49
YSL50	–	IB:YSL40	EB60	–	VIB:B1
PM50	–	IB:PM40	EQ61	D-Quad	VIB:Q1
SK40	–	IB:SK40	EQ62	F-Quad	VIB:Q2
EQ51	D-Quad	IB:Q41	SK62	–	VIB:SK2
EQ52	F-Quad	IB:Q42	BPM62	–	VIB:BPM2
EQ53	D-Quad	IB:Q43	PM62	–	VIB:PM2
EQ54	D-Quad	IB:Q44	EQ63	F-Quad	VIB:Q3
YST50	–	IB:YCB44	EQ64	D-Quad	VIB:Q4
XST50	–	IB:XCB44	EB64	–	VIB:B4
BEM50	–	IB:BEM44	EQ65	D-Quad	VIB:Q5
EQ55	F-Quad	IB:Q45	EQ66	F-Quad	VIB:Q6
SK55	–	IB:SK45	YST66	–	VIB:YCB6
COL55	–	IB:COL45	SK66	–	VIB:SK6
EQ56	D-Quad	IB:Q46	COL66	–	VIB:COL6
EQ57	F-Quad	IB:Q47	FC66	–	VIB:FC6
YST57	–	IB:YCB47	TNIM66	–	VIB:TNIM6
XST57	–	IB:XCB47	PM66	–	VIB:PM6
COL57	–	IB:COL47	XST66	–	VIB:XCB6
FC57	–	IB:FC47			
TNIM57	–	IB:TNIM47			
BPM57	–	IB:BPM47			
PM57	–	IB:PM47			

Table 7: List of optical and diagnostics elements in the horizontal and vertical injection beamline for transporting ion beams from the I1 and I2 terminals.

## 4 Optics modules

### 4.1 Matching section

The matching section consists of four electrostatic quadrupoles and matches the extracted beam from the ion source terminals into the downstream optical modules according to the required Twiss parameters. In our case, the required Twiss parameter alpha is 2.006 and the Twiss parameter beta is 139.3 cm. The calculated beam envelope through this section is shown in Fig. 4 and it is identical for transporting beams from I1 and I2 terminals. The length of this module is about 162.3 cm and the required optical elements in the module are listed in table 8.

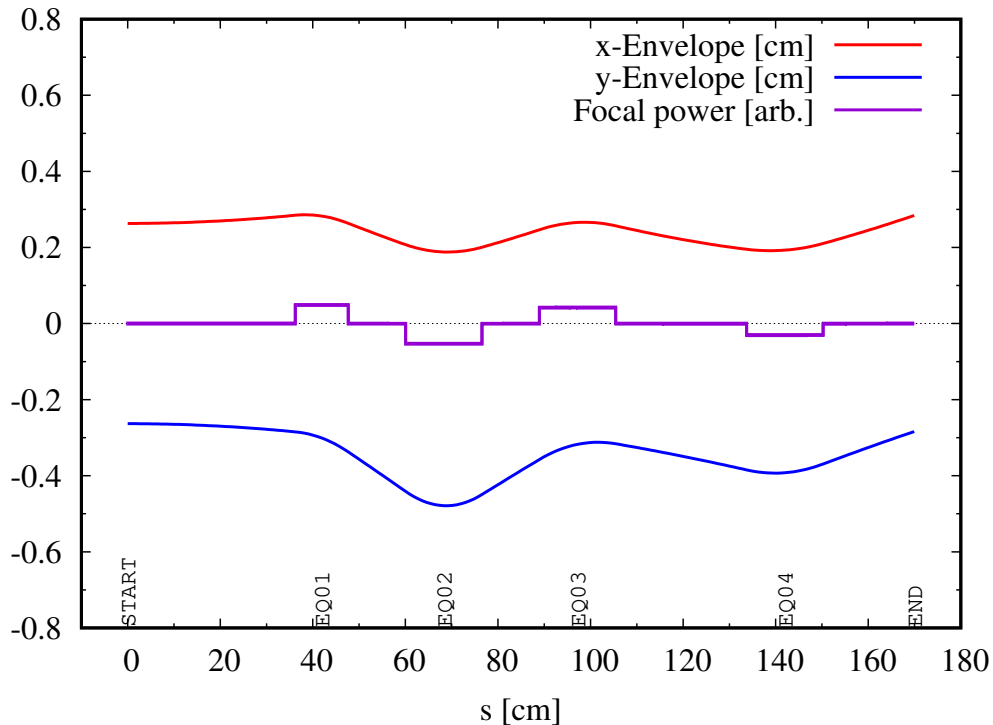


Figure 4: Calculated beam envelope (2RMS, positive for  $x$ , negative for  $y$ ) for a 1 mA of 295 keV  $H^-$  beam transport through a matching section with  $\epsilon_{4rms} = 6 \mu\text{m}$ .

### 4.2 Periodic section

Periodic sections in the horizontal injection beamline are designed to be similar to the periodic section in the vertical beamline [2]. The length of one

Replacement of the ISIS horizontal injection beamline TRI-DN-22-05		
Document-218327	Release No. 02	Release Date: 2022-10-25

Elements	Potential [kV]	$S$ [cm]	$y$ [cm]	$x$ [cm]	$z$ [cm]	$R$ [cm]	$L$ [cm]
START	–	0.0000	0.0000	0.0000	0.0000	–	–
EQ01	3.720	41.9350	0.0000	0.0000	41.9350	2.54	10.16
EQ02	-4.011	68.2950	0.0000	0.0000	68.2950	2.54	15.24
EQ03	3.207	97.1950	0.0000	0.0000	97.1950	2.54	15.24
EQ04	-2.266	141.9830	0.0000	0.0000	141.9830	2.54	15.24
END	–	169.9232	0.0000	0.0000	169.9232	–	–

Table 8: The 4th, 5th and 6th column specifies the reference coordinates of the mid-point of the each quadrupole in the matching section of the injection beamline. Here, START and END are the reference point not a beamline element. The 2nd column specifies the applied voltage to the quadrupoles. The 3rd column ( $S$ ) is the reference trajectory length. Beamline elevation ( $x$ ) reference to the elevation of horizontal injection beamline. The 7th column specifies the aperture radius ( $R$ ) of the quadrupole and 8th column specifies the length ( $L$ ) of the quadrupole.

period is 100 cm and the phase advance per cell is  $45^\circ$  Figure 5 shows the calculated beam envelope through one periodic cell. It consists of two electrostatic quadrupoles with a focal length of 43.7 cm. The coordinates of the optical elements in this module are listed in table 9.

### 4.3 Achromatic bend section

The injection beamline layout consists of two  $90^\circ$  achromatic bend sections. One is in the horizontal plane for transporting the beams from I1 terminal and the other bend section is in the vertical plane that connects the horizontal injection beamline with the vertical injection beamline. Each bend section consists of two  $45^\circ$  cylindrical type electrostatic benders along eight electrostatic quadrupoles as listed in table 10 and 11. Figure 6 shows the calculated beam envelope through the achromatic section in the horizontal plane, whereas Fig 7 shows the calculated beam envelope for the achromatic section in the vertical plane. The optical elements in both achromatic sections are identical except for the polarity of the quadrupoles and quadrupole in the exit of the vertical bend section. The quadrupoles EQ07 and EQ08 in the vertical bend section are optimized to match the beam into the downstream periodic in the vertical injection beamline (See Fig. 7).

Replacement of the ISIS horizontal injection beamline TRI-DN-22-05		
Document-218327	Release No. 02	Release Date: 2022-10-25

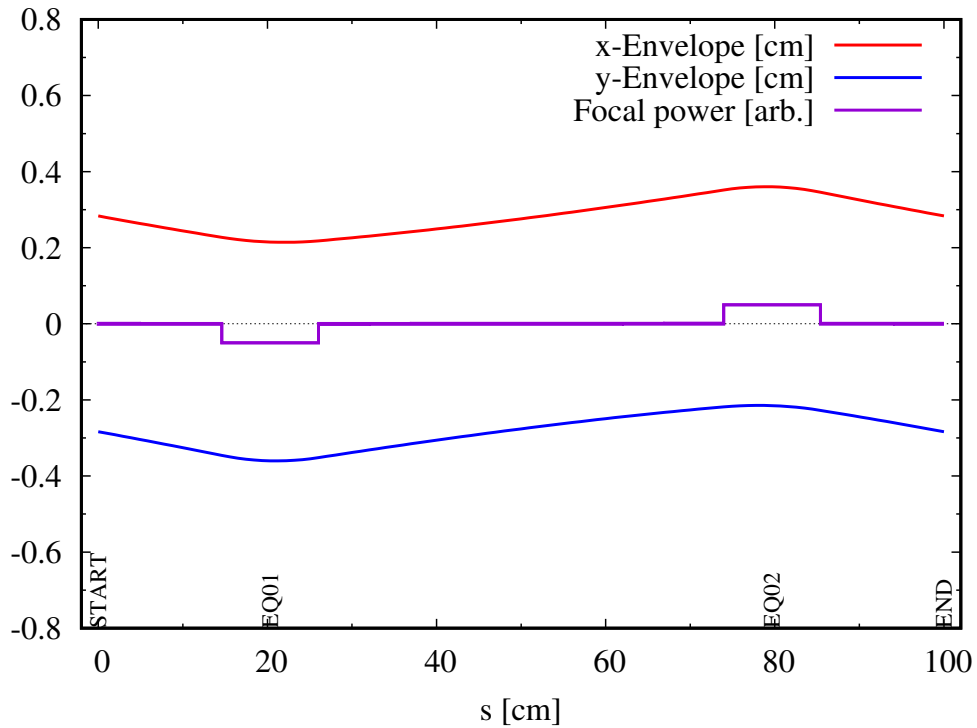


Figure 5: Calculated beam envelope (2RMS, positive for  $x$ , negative for  $y$ ) for a 1 mA of 295 keV  $H^-$  beam transport through a periodic section with  $\varepsilon_{4rms} = 6 \mu\text{m}$ .

Elements	Potential [kV]	$S$ [cm]	$y$ [cm]	$x$ [cm]	$z$ [cm]	$R$ [cm]	$L$ [cm]
START	–	0.0000	0.0000	0.0000	0.0000	–	–
EQ01	-3.806	20.3200	0.0000	0.0000	20.3200	2.54	10.16
EQ02	3.806	79.6800	0.0000	0.0000	79.6800	2.54	10.16
END	–	100.0000	0.0000	0.0000	100.0000	–	–

Table 9: The 4th, 5th and 6th column specifies the reference coordinates of the mid-point of the each quadrupole in the periodic section of the injection beamline. The 2nd column specifies the applied voltage to the quadrupoles. The 3rd column ( $S$ ) is the reference trajectory length. Beamline elevation ( $x$ ) reference to the elevation of horizontal injection beamline. The 7th column specifies the aperture radius ( $R$ ) of the quadrupole and 8th column specifies the length ( $L$ ) of the quadrupole.

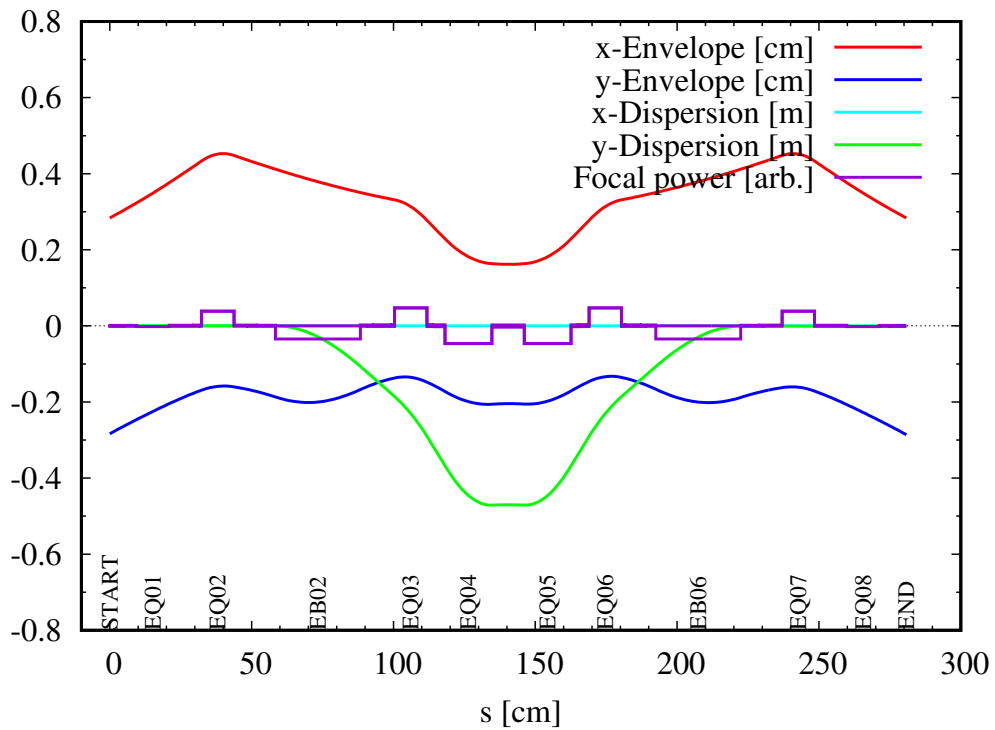


Figure 6: Calculated beam envelope (2RMS, positive for  $x$ , negative for  $y$ ) for a 1 mA of 295 keV  $H^-$  beam transport through a horizontal bend section with  $\varepsilon_{4rms} = 6 \mu\text{m}$ .

Replacement of the ISIS horizontal injection beamline TRI-DN-22-05		
Document-218327	Release No. 02	Release Date: 2022-10-25

Elements	Potential [kV]	$S$ [cm]	$y$ [cm]	$x$ [cm]	$z$ [cm]	$R$ [cm]	$L$ [cm]
START	–	0.0000	0.0000	0.0000	0.0000	–	–
EQ01	-0.145	15.2200	0.0000	0.0000	15.2200	2.54	10.16
EQ02	2.935	38.0800	0.0000	0.0000	38.0800	2.54	10.16
EB02	30.237, -28.762	73.3619	-2.9002	0.0000	72.9802	–	–
EQ03	3.591	106.1037	-23.7316	0.0000	97.9131	2.54	10.16
EQ04	-3.530	126.4237	-38.1000	0.0000	112.2815	2.54	15.24
EQ05	-3.530	154.3637	-57.8566	0.0000	132.0381	2.54	15.24
EQ06	3.591	174.6837	-72.2250	0.0000	146.4065	2.54	10.16
EB06	30.237, -28.762	207.4256	-97.1579	0.0000	167.2379	–	–
EQ07	2.935	242.7074	-132.0581	0.0000	170.1381	2.54	10.16
EQ08	-0.145	265.5674	-154.9181	0.0000	170.1381	2.54	10.16
END	–	280.7874	-170.1381	0.0000	170.1381	–	–

Table 10: The 4th, 5th and 6th column specifies the reference coordinates of the mid-point of the each quadrupole in the horizontal bend section of the injection beamline. The 2nd column specifies the applied voltage to the quadrupoles. The 3rd column ( $S$ ) is the reference trajectory length. Beam-line elevation ( $x$ ) reference to the elevation of horizontal injection beamline. The 7th column specifies the aperture radius ( $R$ ) of the quadrupole and 8th column specifies the length ( $L$ ) of the quadrupole.

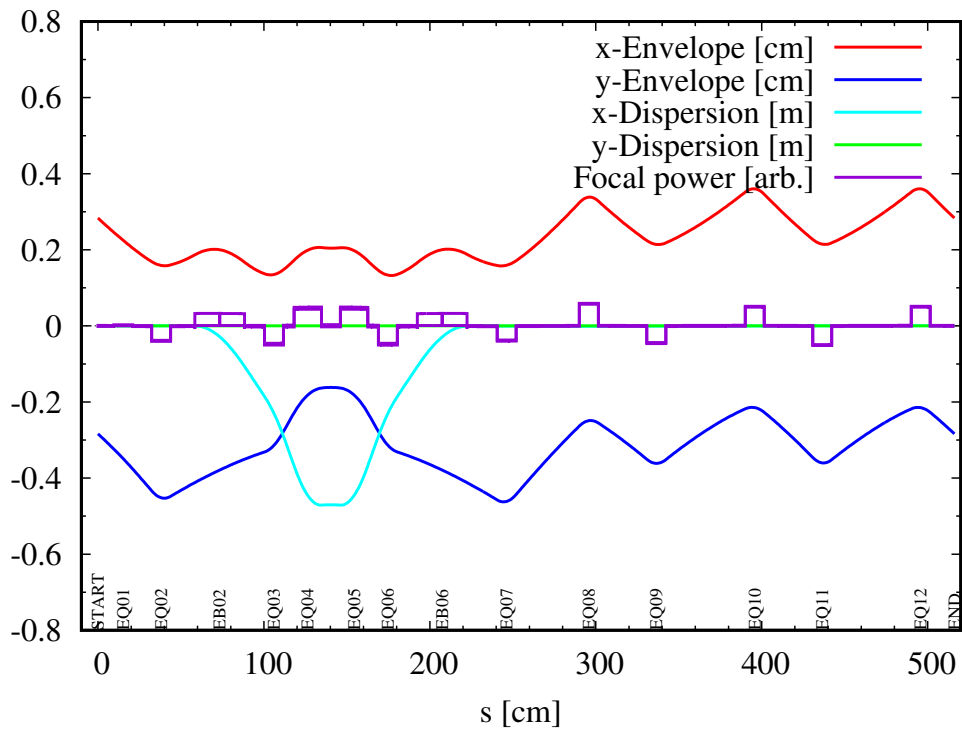


Figure 7: Calculated beam envelope (2RMS, positive for  $x$ , negative for  $y$ ) for a 1 mA of 295 keV  $H^-$  beam transport through a vertical bend section with  $\varepsilon_{4rms} = 6 \mu\text{m}$ .

Replacement of the ISIS horizontal injection beamline TRI-DN-22-05		
Document-218327	Release No. 02	Release Date: 2022-10-25

Elements	Potential [kV]	$S$ [cm]	$y$ [cm]	$x$ [cm]	$z$ [cm]	$R$ [cm]	$L$ [cm]
START	–	0.0000	0.0000	0.0	0.0000	–	–
EQ01	0.145	15.2199	0.0000	0.0	15.2200	2.54	10.16
EQ02	-2.935	38.0799	0.0000	0.0	38.0799	2.54	10.16
EB02	30.237, -28.762	73.3618	-2.9001	0.0	72.9802	2.54	10.16
EQ03	-3.591	106.1036	-23.7315	0.0	97.9131	2.54	10.16
EQ04	3.530	126.4236	-38.1000	0.0	112.2815	2.54	15.24
EQ05	3.530	154.3640	-57.8565	0.0	132.0382	2.54	15.24
EQ06	-3.591	174.6844	-72.2250	0.0	146.4066	2.54	10.16
EB06	30.237, -28.762	207.4263	-97.1579	0.0	167.2380	2.54	10.16
EQ07	-2.894	246.2772	-135.6271	0.0	170.1383	2.54	10.16
EQ08	4.415	295.8316	-185.1802	0.0	170.1383	2.54	10.16
EQ09	-3.408	336.4708	-225.8200	0.0	170.1383	2.54	10.16
EQ10	3.806	395.8306	-285.1798	0.0	170.1383	2.54	10.16
EQ11	-3.806	436.4698	-325.8199	0.0	170.1383	2.54	10.16
EQ12	3.806	495.8297	-385.1798	0.0	170.1383	2.54	10.16
PM00	–	516.1497	-405.4998	0.0	170.1383	–	–

Table 11: The 4th, 5th and 6th column specifies the reference coordinates of the mid-point of the each quadrupole in the vertical bend section of the injection beamline. The 2nd column specifies the applied voltage to the quadrupoles. The 3rd column ( $S$ ) is the reference trajectory length. Beam-line elevation ( $x$ ) reference to the elevation of horizontal injection beamline. The 7th column specifies the aperture radius ( $R$ ) of the quadrupole and 8th column specifies the length ( $L$ ) of the quadrupole.

## 4.4 Five-to-one selector

The calculated beam envelope for the optics 5:1 selector with a periodic section at the entrance is shown in Fig. 8. The length of this module is about 500 cm including a periodical section. This module has been designed to accommodate the buncher, high energy pulser, 5:1 selector and x/y slits. The proposed location for these devices is shown in the envelope and also listed in table 12 along with the location of the quadrupoles. The 2RMS beam size at the slit location is about 1 mm in the vertical plane ( $x$ ) and about 7 mm in the horizontal plane ( $y$ ). Hence, the high energy pulser and the 5:1 selector will be installed in such a way that it kicks the transported beam along the vertical plane.

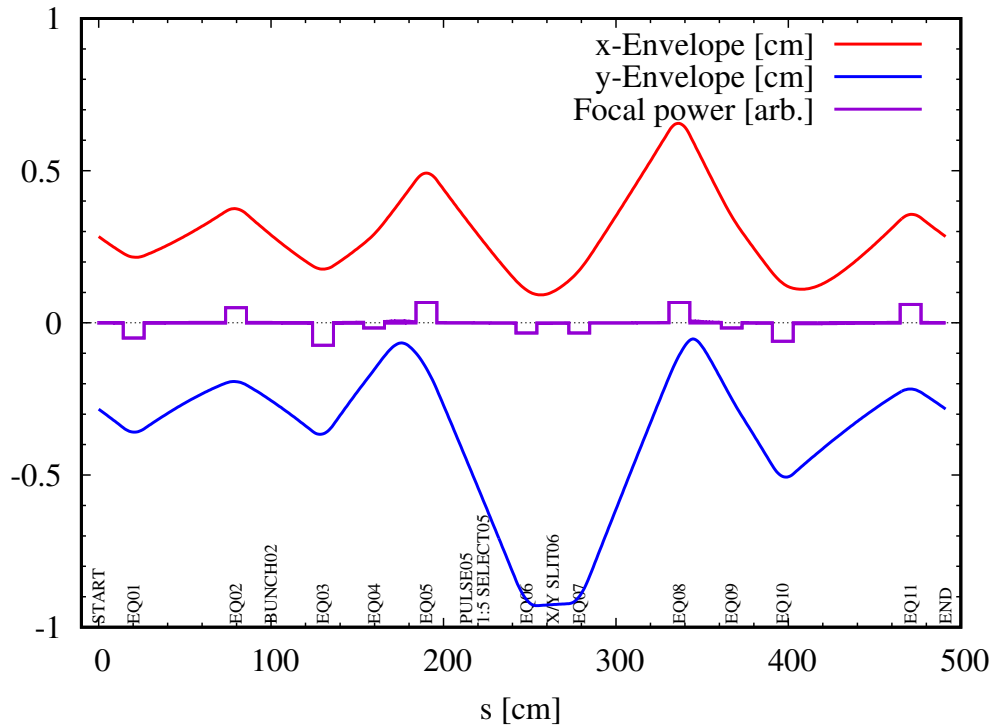


Figure 8: Calculated beam envelope (2RMS, positive for  $x$ , negative for  $y$ ) for a 1 mA of 295 keV  $H^-$  beam transport through a low beta insertion with  $\varepsilon_{4rms} = 6 \mu m$ .

Replacement of the ISIS horizontal injection beamline TRI-DN-22-05		
Document-218327	Release No. 02	Release Date: 2022-10-25

Elements	Potential [kV]	$S$ [cm]	$y$ [cm]	$x$ [cm]	$z$ [cm]	$R$ [cm]	$L$ [cm]
START		0.0000	0.0	0.0	0.0000	–	–
EQ01	-3.806	20.3199	0.0	0.0	20.3200	2.54	10.16
EQ02	3.806	79.6801	0.0	0.0	79.6800	2.54	10.16
BUNCH02	–	100.0002	0.0	0.0	100.0000	–	–
EQ03	-5.617	130.1303	0.0	0.0	130.1300	2.54	10.16
EQ04	-1.286	159.7469	0.0	0.0	159.7461	2.54	10.16
EQ05	5.072	190.0822	0.0	0.0	190.0809	2.54	10.16
PULSE05	–	219.1022	0.0	0.0	219.1008	–	–
5:1 SELECT05	–	219.1022	0.0	0.0	219.1008	–	–
EQ06	-2.522	248.1223	0.0	0.0	248.1208	2.54	10.16
X/Y SLIT06	–	263.4326	0.0	0.0	263.4308	–	–
EQ07	-2.522	278.7429	0.0	0.0	278.7407	2.54	10.16
EQ08	5.072	336.7825	0.0	0.0	336.7804	2.54	10.16
EQ09	-1.286	367.1174	0.0	0.0	367.1146	2.54	10.16
EQ10	-4.614	396.7330	0.0	0.0	396.7302	2.54	10.16
EQ11	4.614	470.8437	0.0	0.0	470.8394	2.54	10.16
END	–	491.1637	0.0	0.0	491.1594	–	–

Table 12: The 4th, 5th and 6th column specifies the reference coordinates of the mid-point of the each quadrupole in the 5:1 selector section of the injection beamline. The 2nd column specifies the applied voltage to the quadrupoles. The 3rd column ( $S$ ) is the reference trajectory length. Beam-line elevation ( $x$ ) reference to the elevation of horizontal injection beamline. The 7th column specifies the aperture radius ( $R$ ) of the quadrupole and 8th column specifies the length ( $L$ ) of the quadrupole.

Replacement of the ISIS horizontal injection beamline TRI-DN-22-05		
Document-218327	Release No. 02	Release Date: 2022-10-25

## 4.5 The beam bunching

The bunchers in the injection beamline are used to modulate the velocity of the dc beam such that the beam becomes bunched at the injection point. At present there are two double gap bunchers being used in the injection beamline. The first buncher is installed at the horizontal injection beamline at a distance 21 m from the injection and the 2nd buncher is located 4.54 m downstream of the 1st buncher. The 1st buncher operates at the cyclotron RF frequency (23.06 MHz) while the other operates at the second harmonic (46.12 MHz). The reported bunching efficiency of this system is about 57% at 490  $\mu\text{A}$  injection line current corresponds to 245  $\mu\text{A}$  extracted current from the cyclotron [8]. As part of the horizontal injection beamline upgrade, the present buncher system will be replaced with a new buncher system.

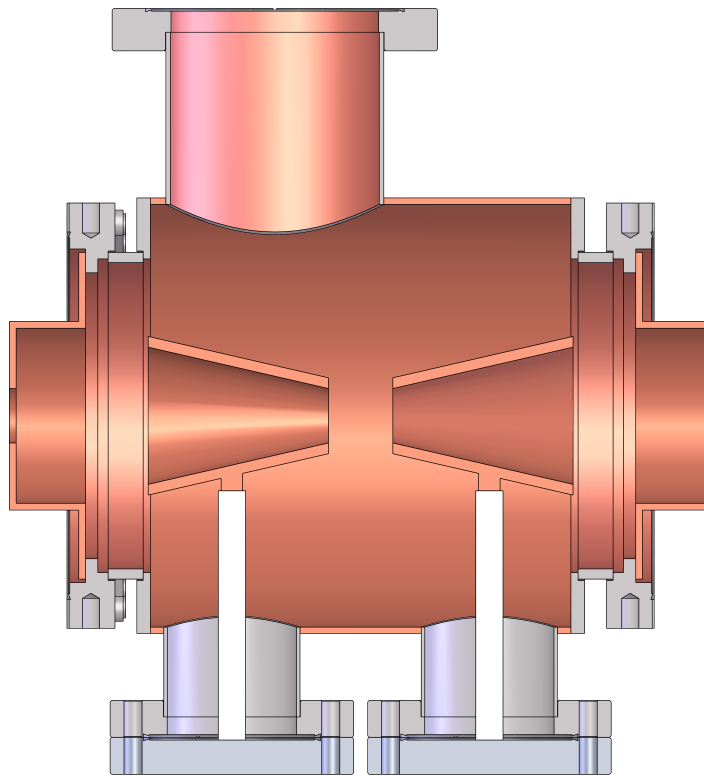


Figure 9: Proposed 3D model of the multi-harmonic buncher.

Replacement of the ISIS horizontal injection beamline TRI-DN-22-05		
Document-218327	Release No. 02	Release Date: 2022-10-25

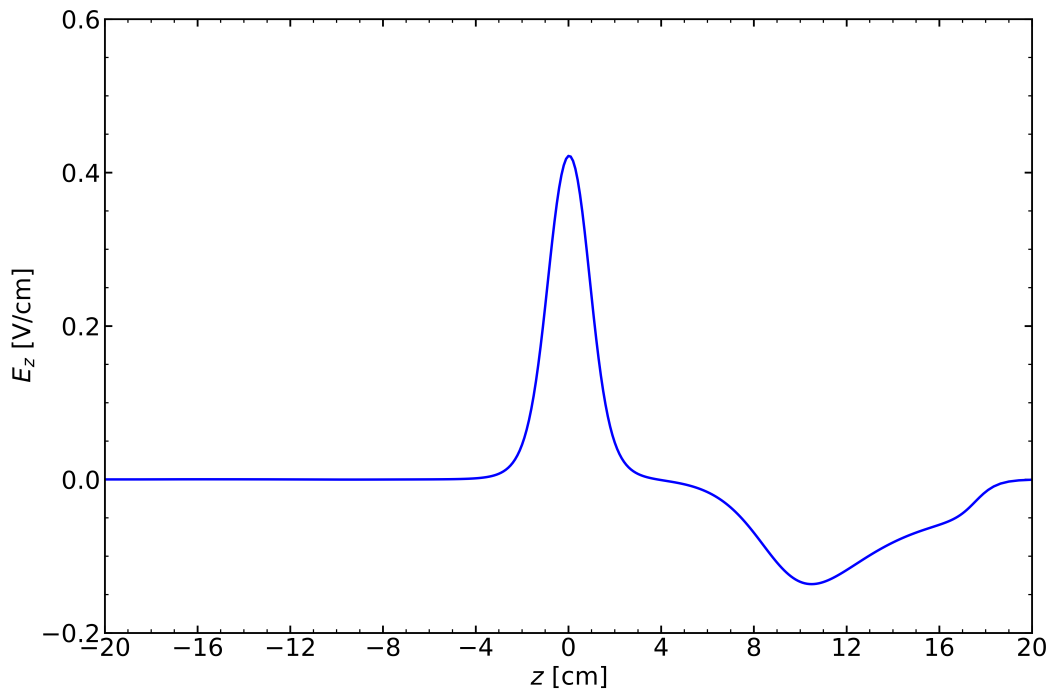


Figure 10: Calculated electric field ( $E_z$ ) along the axis of the buncher with an applied potential of 1 V.

A two electrode multi-harmonic buncher system has been designed with a 12.7 mm aperture radius and a 15 mm gap between the electrodes [9]. The layout of the buncher system is shown in Fig. 9. The particle tracking code WARP3D [10] was used in an earlier work to simulate the longitudinal beam dynamics for the existing buncher system in the injection beamline [11]. In this work also, the WARP3D code has been chosen to study the performance of the multi-harmonic buncher.

The calculated electrostatic field along the axis of the buncher is shown in Fig. 14 and the calculated field map is imported into the particle tracking code WARP3D. The imported field map is then modulated at the first three harmonics of 23.06 MHz. The multi-harmonic buncher is installed at the horizontal injection beamline at a distance 20 m from the injection, which is one metre closer to the injection compared to the existing buncher system. In order to keep the simulation model simple, 20 lattice periods have been assumed between the multi-harmonic buncher and the injection point. Figure 11 shows the calculated transverse (top) and longitudinal (bottom) beam envelope through these lattice periods including the space-charge effects, by using the code WARP3D. Figure 12 shows the calculated transverse phase-space at the injection point and Fig. 13 shows the calculated longitudinal space at the same location. The initial beam intensity in this case is 200  $\mu\text{A}$ .

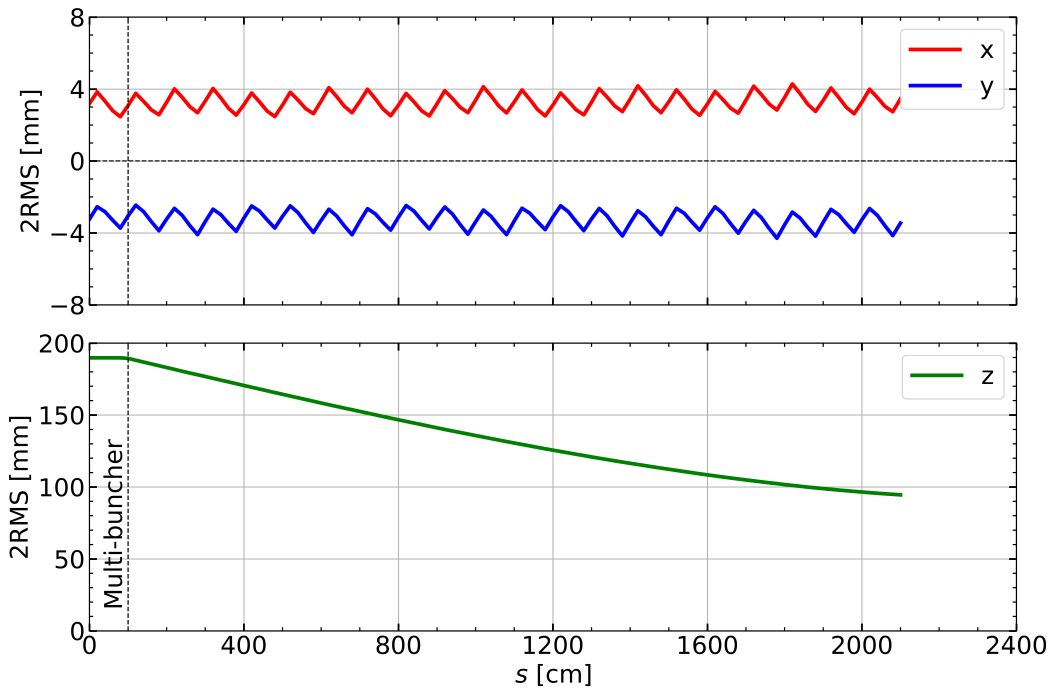


Figure 11: Calculated beam envelope (2RMS, positive for  $x$ , negative for  $y$ , longitudinal for  $z$ ) for a  $200 \mu\text{A}$  of  $300 \text{ keV H}^-$  beam transport through 21 periodical lattice and buncher with  $\epsilon_{4\text{rms}} = 8 \mu\text{m}$ .

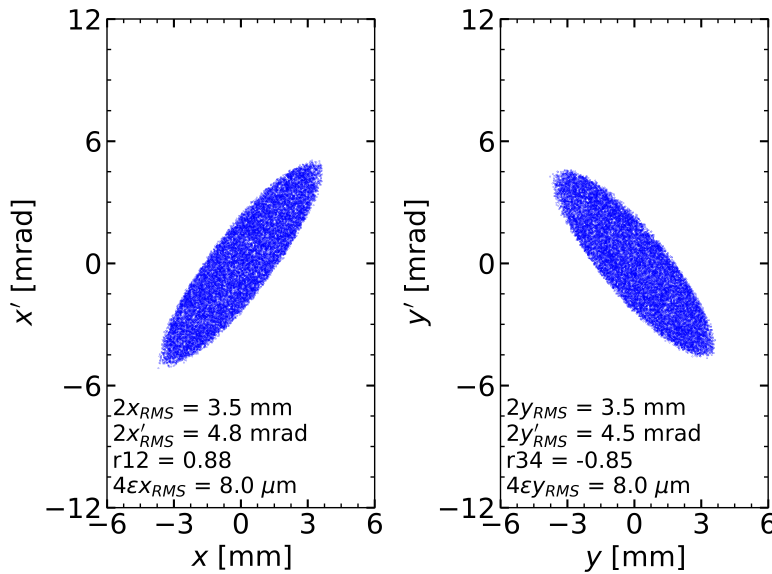


Figure 12: Calculated transverse phase-space of the  $300 \text{ keV H}^-$  beam with an initial beam intensity of  $200 \mu\text{A}$  with the multi-harmonic buncher.

Replacement of the ISIS horizontal injection beamline TRI-DN-22-05		
Document-218327	Release No. 02	Release Date: 2022-10-25

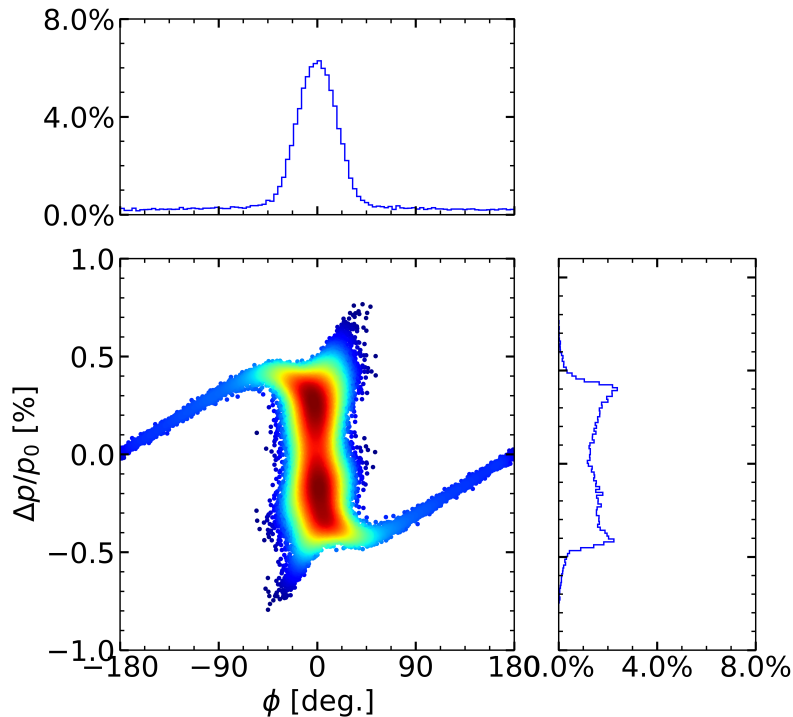


Figure 13: Calculated longitudinal phase-space of the 300 keV  $H^-$  beam with an initial beam intensity of 200  $\mu A$  with the multi-harmonic buncher. About 64.8% particles are within the phase acceptance of  $\pm 25^\circ$  and momentum spread ( $\Delta p/p$ ) of  $\pm 0.5\%$ .

In order to improve the bunching efficiency in the case of higher beam intensity, in particular above 500  $\mu A$  the buncher needs to be located closer to the injection point compared to in the case of 200  $\mu A$ . As moving the position of the buncher along the beamline is impractical for various beam intensity an additional 1st harmonic buncher (re-buncher) 13.5 m away from the multi-harmonic buncher has been included as a re-buncher in the simulation in the case of beam intensity higher than 500  $\mu A$ . The calculations show that adding an additional 1st harmonic buncher (re-buncher) 13.5 m away from the multi-harmonic buncher improves the bunching efficiency for the beam intensity higher than 500  $\mu A$ . Figure 16 shows the calculated transverse phase-space at the injection point and Fig. 17 shows the calculated longitudinal space at the same location. Initial beam intensity in this case is 1 mA. Fig. 18 shows the calculated longitudinal space with an initial beam intensity of 650  $\mu A$ . The bunching efficiency of this system is about 66% at 650  $\mu A$  injection line current corresponds to 429  $\mu A$  extracted currents are expected from the cyclotron for assuming a phase acceptance of  $\pm 25^\circ$  and momentum spread ( $\Delta p/p$ ) of  $\pm 0.5\%$ .

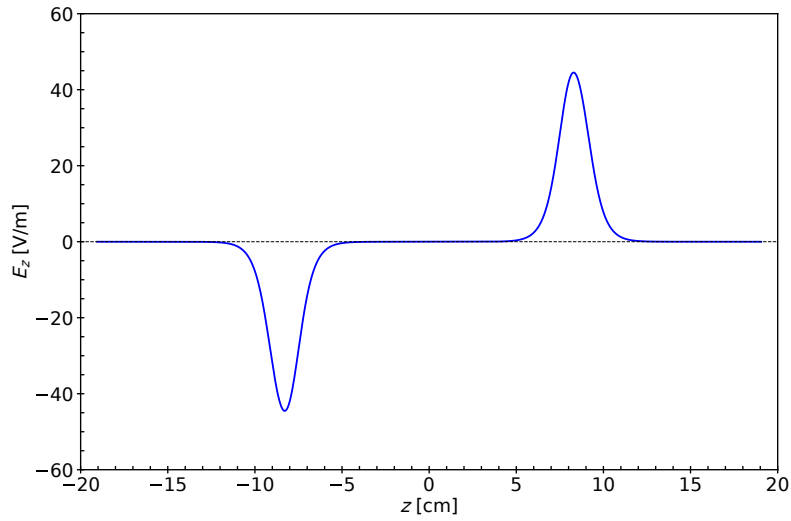


Figure 14: Calculated electric field ( $E_z$ ) along the axis of the buncher with an applied potential of 1 V.

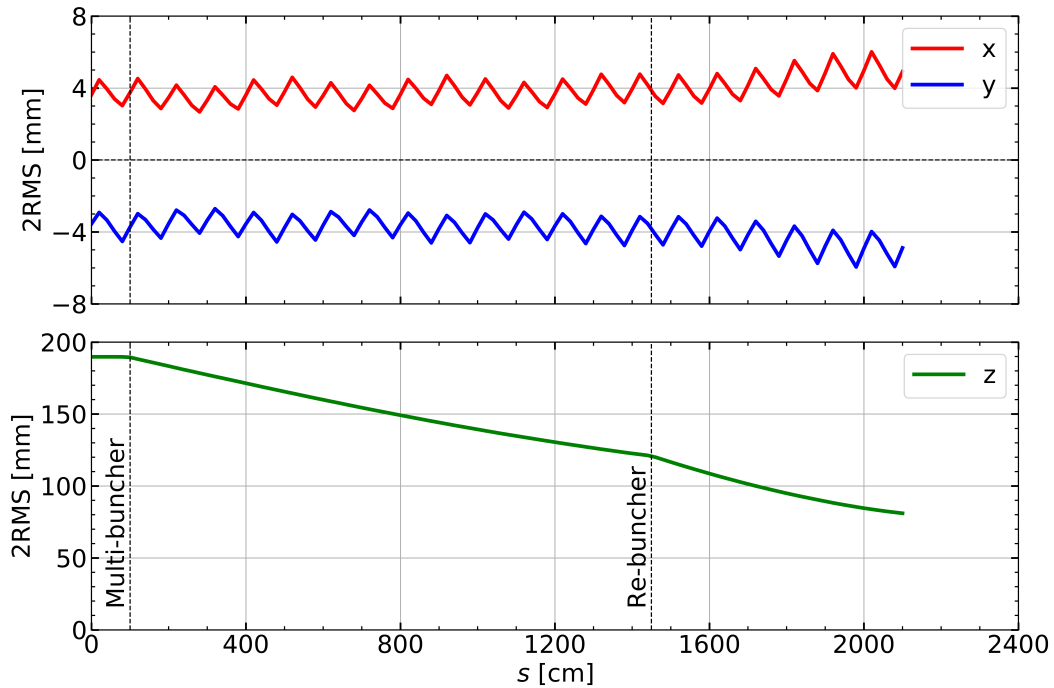


Figure 15: Calculated beam envelope (2RMS, positive for  $x$ , negative for  $y$ , longitudinal for  $z$ ) for a 1 mA of 300 keV  $H^-$  beam transport through 21 periodical lattice and buncher with  $\epsilon_{4rms} = 8 \mu m$ .

Replacement of the ISIS horizontal injection beamline TRI-DN-22-05		
Document-218327	Release No. 02	Release Date: 2022-10-25

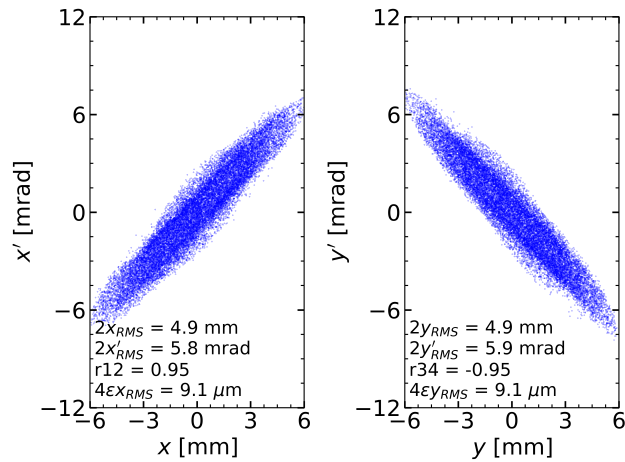


Figure 16: Calculated transverse phase-space of the 300 keV  $H^-$  beam with an initial beam intensity of 1 mA with the multi-harmonic buncher and the re-buncher.

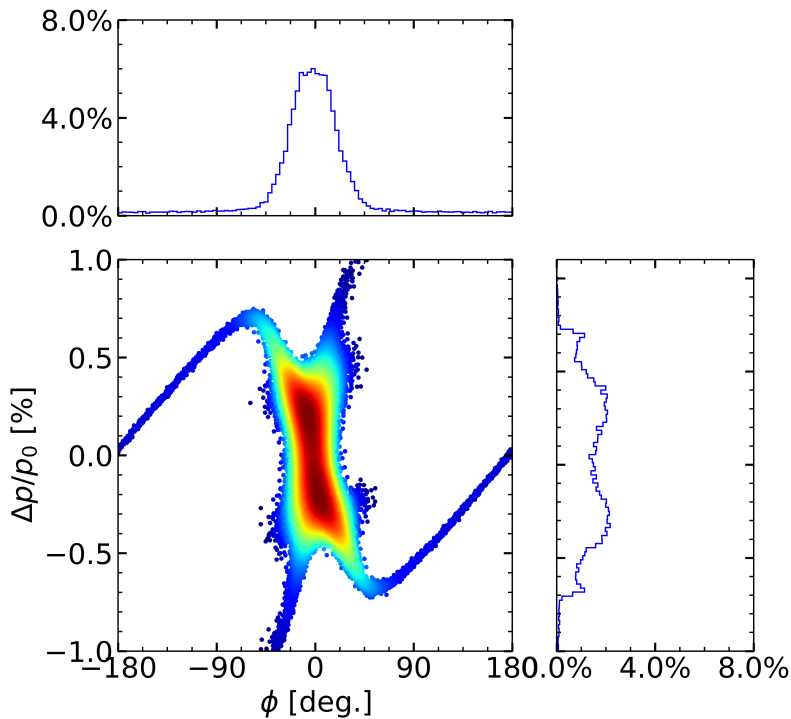


Figure 17: Calculated longitudinal phase-space of the 300 keV  $H^-$  beam with an initial beam intensity of 1 mA with the multi-harmonic buncher and the re-buncher. About 63.8% particles are within the phase acceptance of  $\pm 25^\circ$  and momentum spread ( $\Delta p/p$ ) of  $\pm 0.5\%$ .

Replacement of the ISIS horizontal injection beamline TRI-DN-22-05		
Document-218327	Release No. 02	Release Date: 2022-10-25

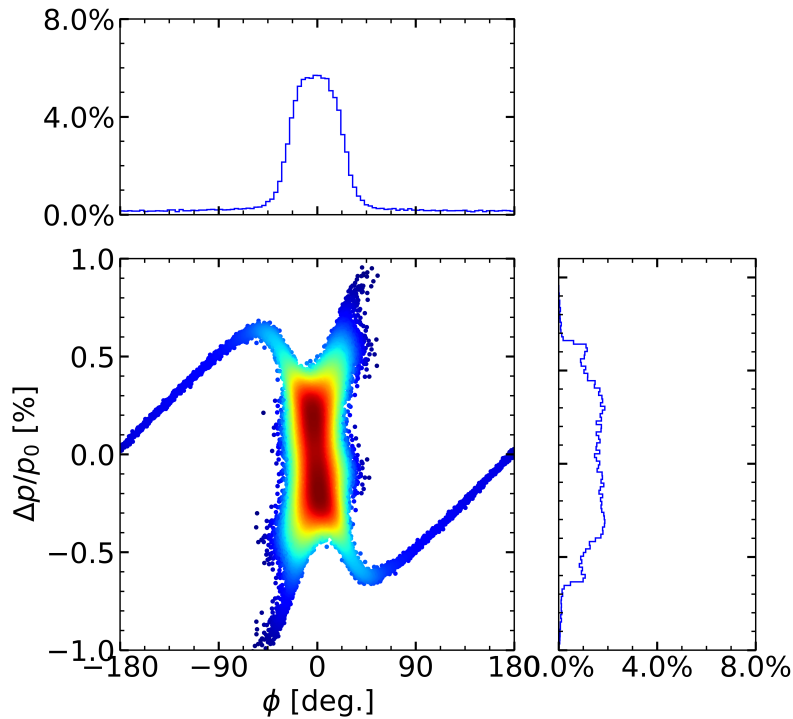


Figure 18: Calculated longitudinal phase-space of the 300 keV  $H^-$  beam with an initial beam intensity of  $650 \mu A$  with the multi-harmonic buncher and the re-buncher. About 66.1% particles are within the phase acceptance of  $\pm 25^\circ$  and momentum spread ( $\Delta p/p$ ) of  $\pm 0.5\%$ .

## 5 Optical elements

### 5.1 Electrostatic quadrupole

The primary focusing elements in the beamline are the electrostatic quadrupoles with an aperture radius of 2.54 cm with two different lengths, 10.16 cm and 15.24 cm. The geometry of an electrostatic quadrupole with its dimensions is shown in Fig 19. Here, the quadrupoles are designed according to the quadrupole geometry proposed in Ref. [7]. Figure 20 shows the calculated potential contour map at the center of the quadrupole by using the code OPERA and Fig. 21 shows the calculated potential through the quadrupole at  $x = 0.254$  cm and  $y = 0$  cm.

Replacement of the ISIS horizontal injection beamline TRI-DN-22-05		
Document-218327	Release No. 02	Release Date: 2022-10-25

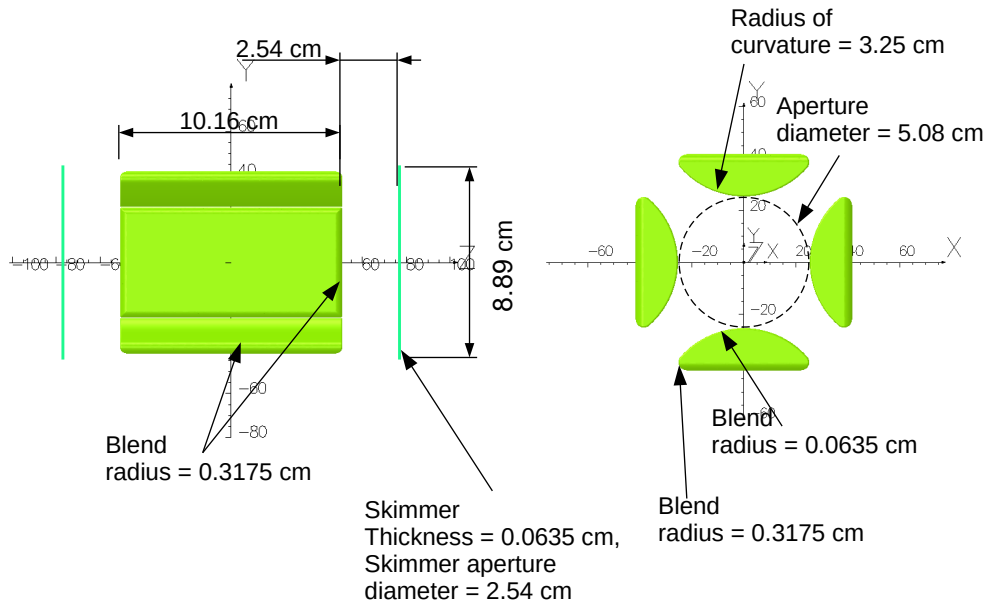


Figure 19: A geometrical view of a electrostatic quadrupole with dimensions.

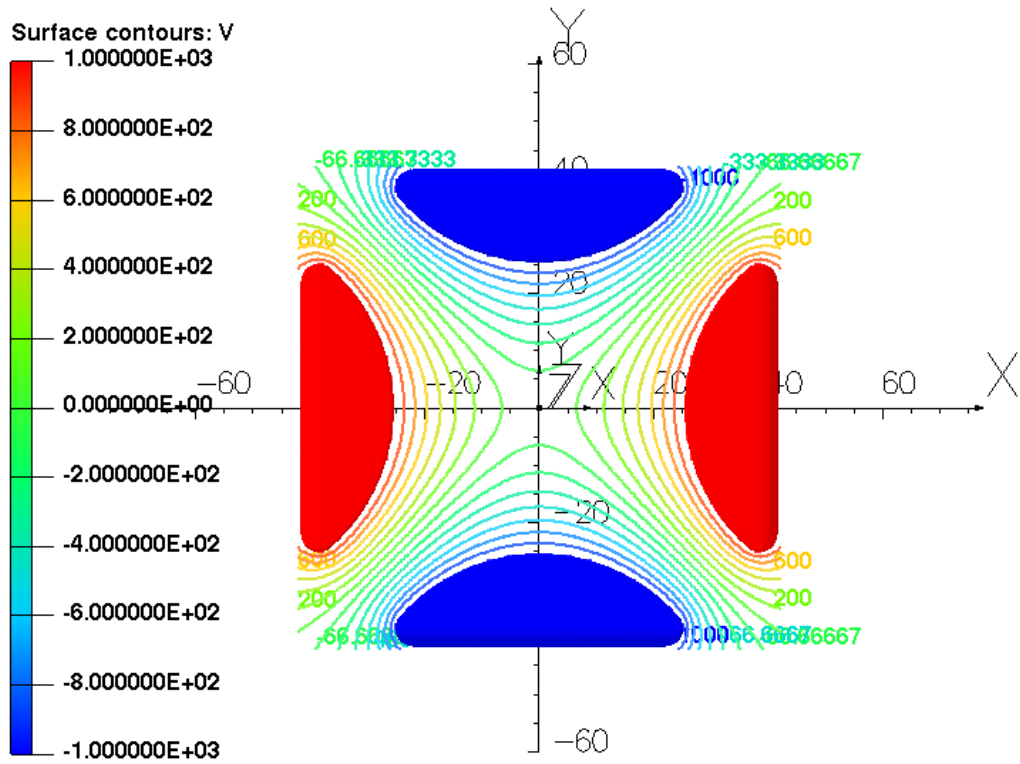


Figure 20: Calculated potential contour map along the  $xy$ -plane at  $z = 0$  cm.

Replacement of the ISIS horizontal injection beamline TRI-DN-22-05		
Document-218327	Release No. 02	Release Date: 2022-10-25

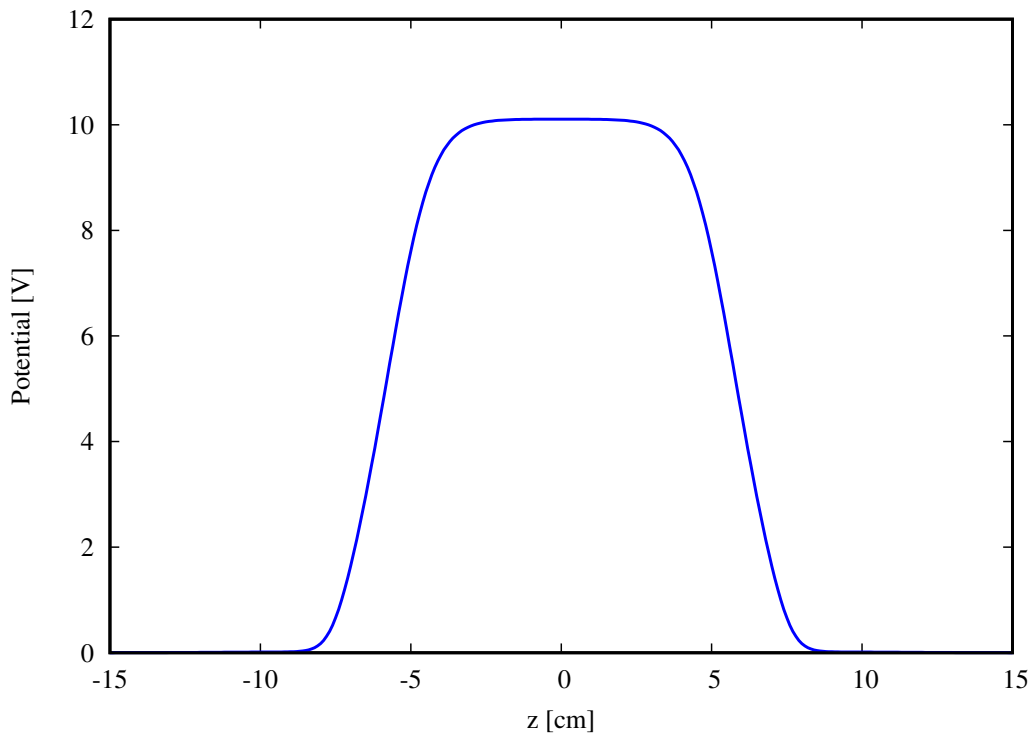


Figure 21: Calculated potential through the quadrupole at  $x = 0.254$  cm and  $y = 0$  cm.

## 5.2 Electrostatic bender

Each  $90^\circ$  achromatic bend section consists of two  $45^\circ$  benders with a bending radius of 38.1 cm. The geometry of the bender and its dimensions are shown in Fig. 22. Figure 23 shows the calculated potential contour map at the center of the bender along the non-bend plane using the code OPERA and Fig. 27 shows the calculated electric field along the reference trajectory through the bender.

Replacement of the ISIS horizontal injection beamline TRI-DN-22-05		
Document-218327	Release No. 02	Release Date: 2022-10-25

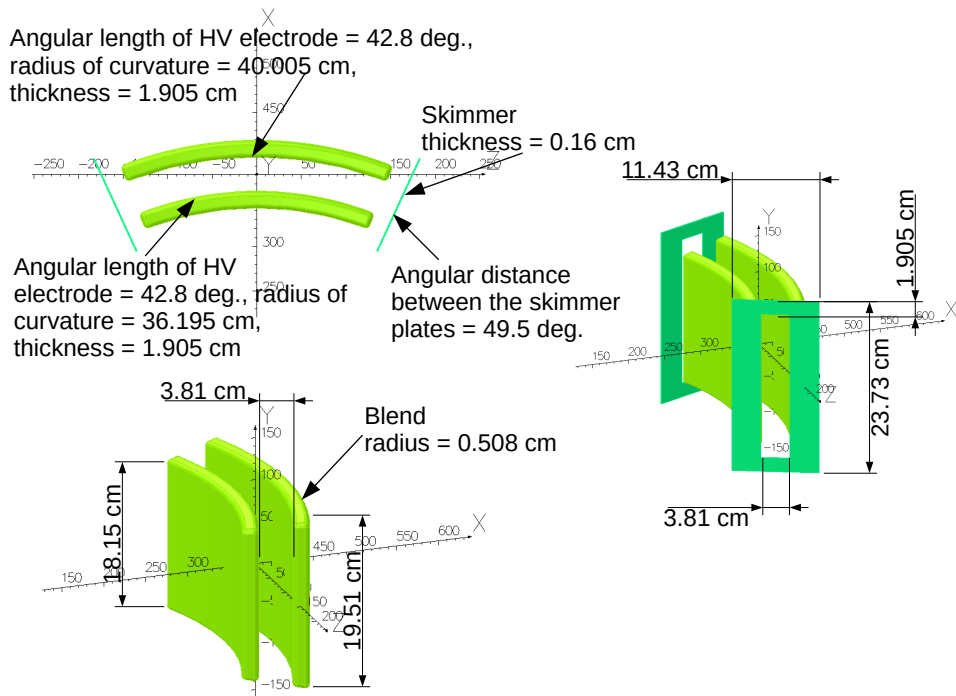


Figure 22: A geometrical view of a 45° electrostatic bender with dimensions.

Replacement of the ISIS horizontal injection beamline TRI-DN-22-05		
Document-218327	Release No. 02	Release Date: 2022-10-25

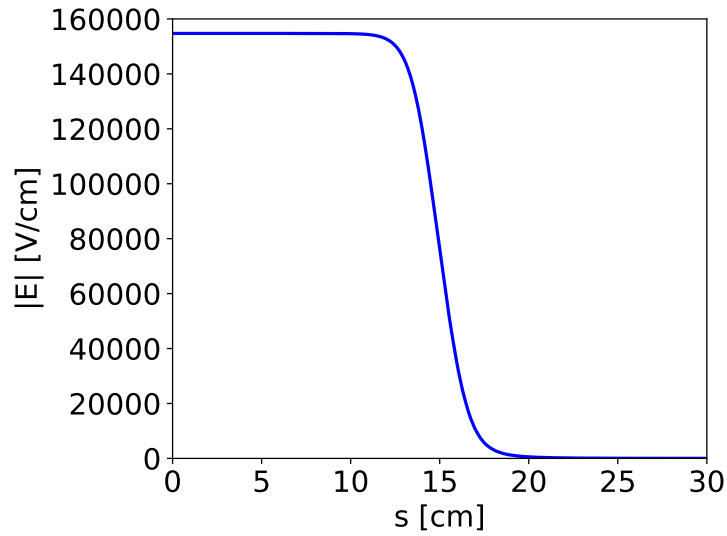


Figure 24: Calculated electric field along the reference trajectory through the  $45^\circ$  electrostatic bender from the center of the bender through the exit of the bender.

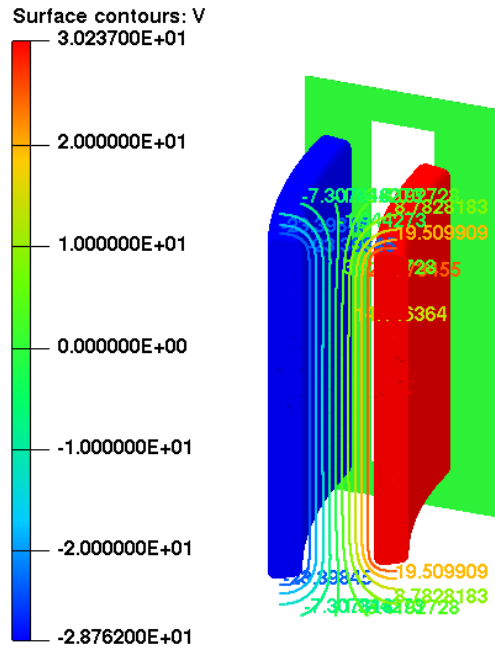


Figure 23: Calculated potential contour map along the  $xy$ -plane at  $z = 0$  cm.

Replacement of the ISIS horizontal injection beamline TRI-DN-22-05		
Document-218327	Release No. 02	Release Date: 2022-10-25

### 5.3 Electrostatic steerer

The geometry of an electrostatic steerer with its dimensions is shown in Fig. 25. Figure 26 shows the calculated potential map of the steerer and skimmer electrodes using the code OPERA and Fig. 27 shows the calculated electric field along the axis of the steerer. A pair of steerers will be installed with a phase-advance about  $90^\circ$  apart along the beamline for orbit correction both in horizontal and vertical planes. Required steerers are listed in table 4, 6 & 7.

The deflection angle ( $\theta_E$ ) by an electrostatic steerer:

$$\theta_E = \frac{V L_E}{2V_E g} = 4.5 \text{ mrad} \quad (1)$$

with  $L_E = 5.08 \text{ cm}$  is effective length, electrode gap  $g = 3.81 \text{ cm}$ , applied potential difference across electrode  $V = 2 \text{ kV}$  and beam voltage  $V_E = 295 \text{ kV}$ .

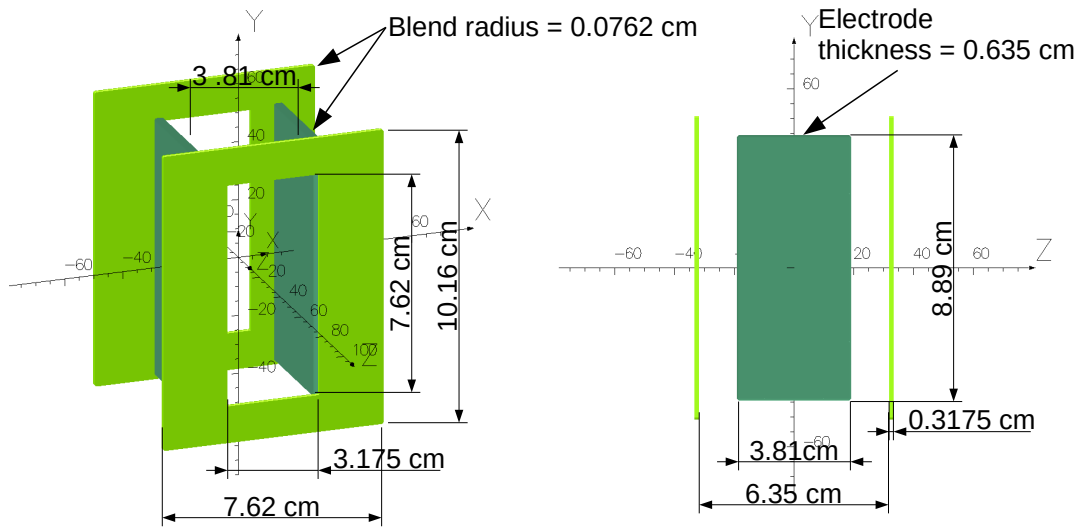


Figure 25: A geometrical view of an electrostatic steerer with dimensions.

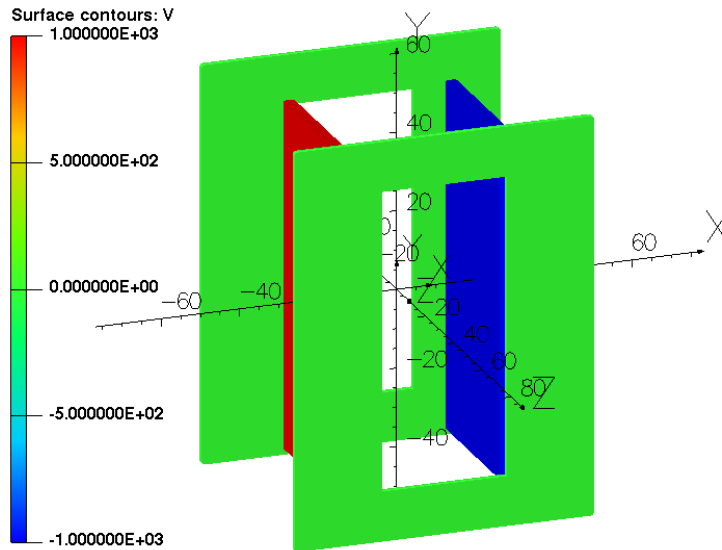


Figure 26: Calculated potential contour map on the surface of the steerer and skimmer electrodes for an applied potential of  $\pm 1000$  V.

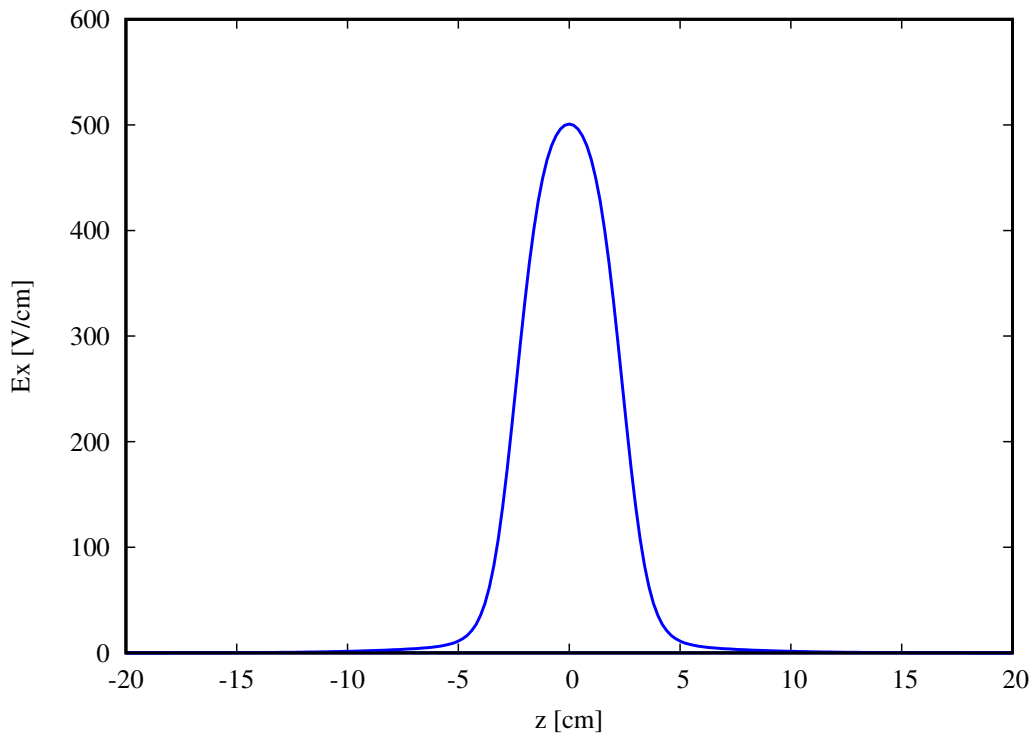


Figure 27: Calculated electric field ( $E_x$ ) along the axis of the steerer for an applied potential of  $\pm 1000$  V.

## 6 Cyclotron stray field compensation

The cyclotron stray magnetic field has been measured at the injection beam line level, and result are included in the TRI-BN-21-14 beam note [12]. The measurements are consistent with the theoretical model of a single coil loop of radius of 8.8 m running a current of 550 kA [13], as represented in figure 28; spikes in the measurement data are attributed to soft steel elements in the existing beamline.

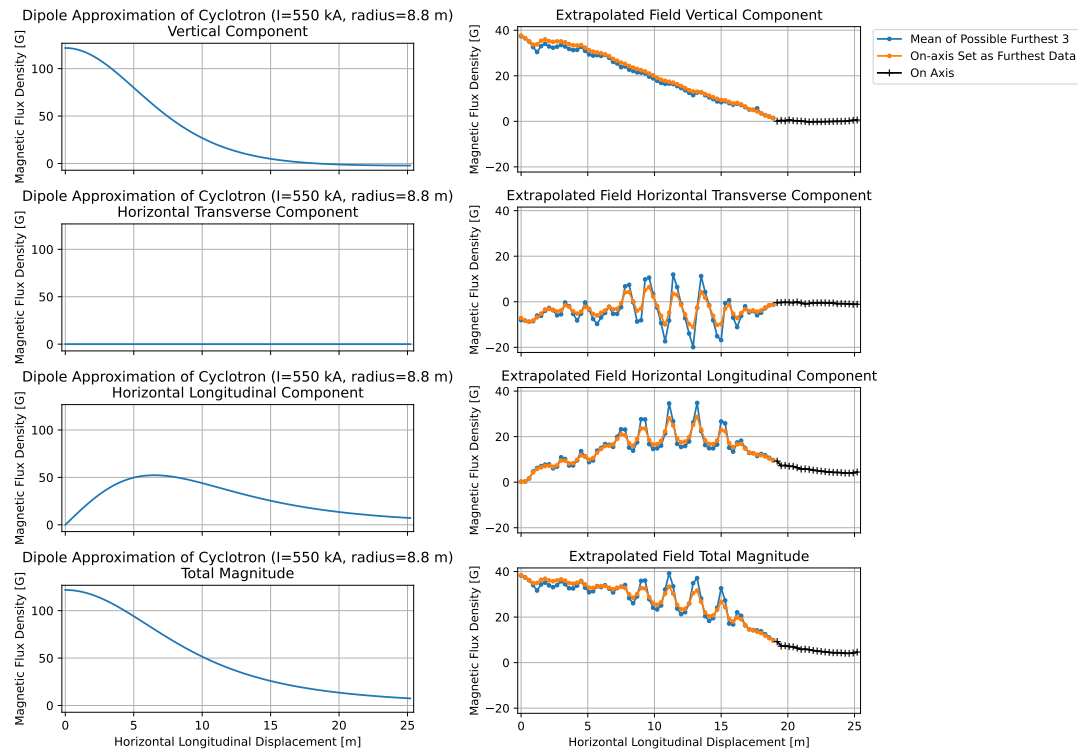


Figure 28: Theoretical stray magnetic field (left) and measured one (right) as documented in TRI-BN-21-14 [12]: the horizontal scale represents the distance from vertical injection beamline ( $z=0$ ) along the horizontal section. Trends of measured data match expectation: spikes in the measurements are attributed to soft steel elements in the existing beamline.

The vertical is the strongest component of the magnetic field, and it reaches a peak of about 35 G close to the vertical injection line. The horizontal components is on average less than 5 G, while the longitudinal one, with a peak of about 20 G, does not significantly effect the beam transverse dynamics.

Replacement of the ISIS horizontal injection beamline TRI-DN-22-05		
Document-218327	Release No. 02	Release Date: 2022-10-25

The transverse components (vertical and horizontal) must be compensated as per requirements [4] in order to avoid beam losses along the beamline. The compensated residual field should be on average below 1 G. Since the 300 keV  $H^-$  has a rigidity of about 792 G·m, a field integral of 1 G·m (calculated over a 1 m long periodic section) will produce a deflection of about 1.3 mrad, which can be compensated with steering elements.

## 6.1 Compensation systems

The compensation strategy considered two systems: a passive one (similar to the existing ISIS soft-steel shielding) and an active one (like the compensation coils in the e-linac system [14]).

The passive compensation system consists of an in-vacuum (internal) 2 mm thick  $\mu$ -metal shielding liners magnetically (and mechanically) connected to each other to form a single shielding unit for the whole length of the beamline, including the diagnostic boxes; this is in fact a limitation of the existing system where the diagnostic boxes create large gaps in the external soft-steel shielding (see figure 7 in [12]). A preliminary design of the in-vacuum system is represented (blue liner) in figure 29; the optical elements (quadrupole and steerers) are located inside the liner.

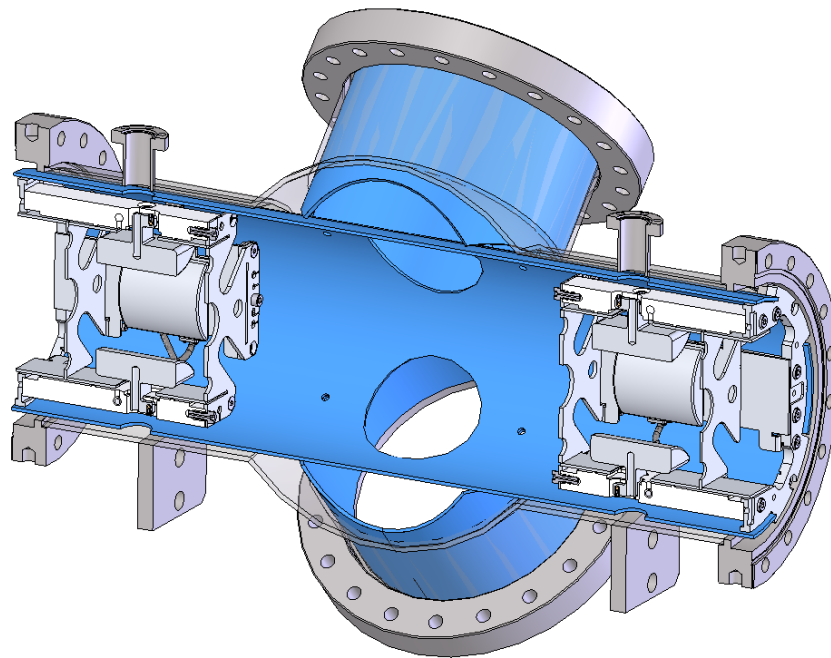


Figure 29: Preliminary design of the  $\mu$ -metal shielding liner (in blue) inside the vacuum chamber. Dedicated openings are implemented for the HV feedthroughs (1.33" CF) and diagnostic devices (8" CF).

Replacement of the ISIS horizontal injection beamline TRI-DN-22-05		
Document-218327	Release No. 02	Release Date: 2022-10-25

Dedicated openings are implemented for the HV feedthroughs and diagnostic devices; the latter openings, being of larger size, are paired with shielding sleeves protruding inside the diagnostic ports of the vacuum chamber to increase the field suppression. Should a diagnostic device not being installed in one of the ports, the opening can be plugged (with a proper  $\mu$ -metal patch) and the corresponding sleeve removed; this of course produces a better field suppression.

The shielding preliminary designed has been simulated in OPERA (see figure 30), as well as two mock-ups with different grade of  $\mu$ -metal have been fabricated (see figure 31), and measured in the cyclotron stray field along the existing horizontal beamline about 1 m eastward close to the vertical section.

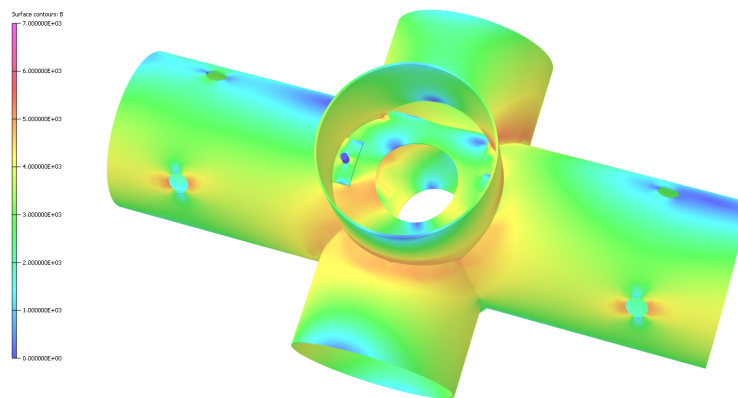


Figure 30: OPERA simulation (field saturation) of a single  $\mu$ -metal liner.



Figure 31: Two mock-ups with identical geometry but different material grade: standard  $\mu$ -metal<sup>®</sup> (left) and Co-NETIC<sup>®</sup>B (right).

Replacement of the ISIS horizontal injection beamline TRI-DN-22-05		
Document-218327	Release No. 02	Release Date: 2022-10-25

The background field used in the OPERA simulations is derived from the background stray field measurement, reported in figure 32, at the beamline location during the mock-up characterization. The chosen simulation background is the maximum value, for each component, of the measured one: horizontal, vertical and longitudinal are respectively  $B_x = -1.3$  G,  $B_y = -38.6$  G and  $B_z = 5.1$  G (signs are as per hall probe orientation during measurements). These values are consistent with the measurements taken earlier (see [12]).

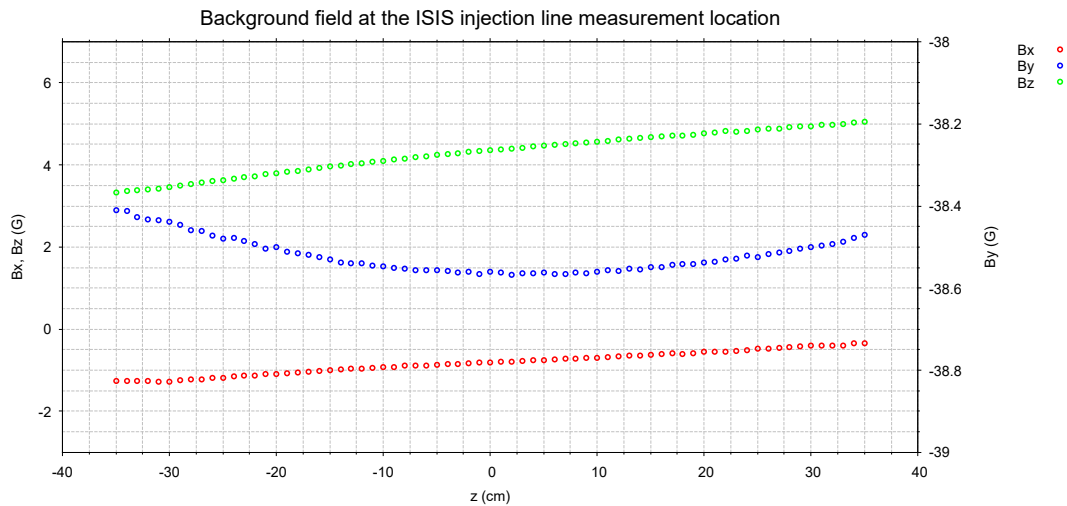


Figure 32: Background stray cyclotron field at the existing horizontal injection beamline location where the mock-up measurements took place (about 1 m east of diagnostic box 165):  $z=0$  corresponds to the center of the mock-up.

The single shielding liner OPERA simulation and the mock-up on-axis measurements are in good agreement, as represented in figure 33, showing an average field suppression to  $< 1$  G, with a peak at the diagnostic port location ( $z=0$  cm), as expected. The  $\mu$ -metal<sup>®</sup> mock-up measurement peaked at about 1.8 G compared to the 1.2 G of the simulation, while the Co-NETIC<sup>®</sup>B mock-up performs slightly better with a peak of 1.5 G.

In both case the difference with respect to the simulation are attributed to the material quality; as a matter of fact the 2 mm wall thickness was reached in both case stacking multiple layers (2 for the  $\mu$ -metal and 3 for the Co-NETIC<sup>®</sup>B) of in house available material.

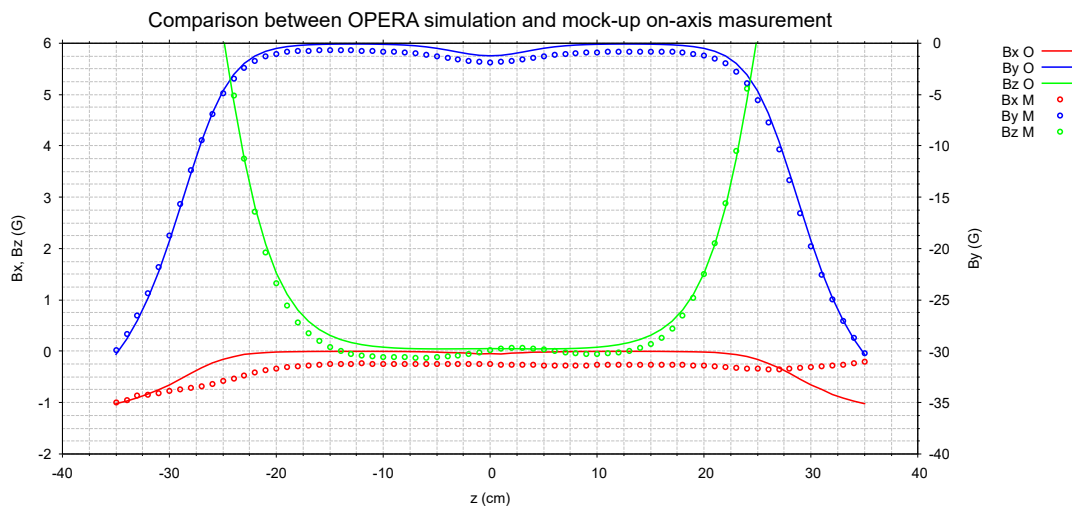


Figure 33: OPERA simulation (O) compared to  $\mu$ -metal mock-up on-axis measurement (M); asymmetries in the  $B_x$  and  $B_z$  are due to the non-uniformity of the real background field for these components (see figure 32), while OPERA uses a constant field. Relevant longitudinal locations:  $z=0$  corresponds to the center of the mock-up and hence the diagnostic port openings,  $z=\pm 20$  correspond to the HV feedthrough openings,  $z=\pm 27$  correspond to the edges of the mock-up.

Additional simulations show that the connections between the sleeves and the main body of the shielding are critical to reduced the peak, which can be further suppressed by decreasing the sleeves diameter. An already revised design implements both smaller diameter and better connections.

A multi-boxes simulation with three adjacent shielding liners (see figure 34) shows that even a 5 mm gap does not compromise the suppression of the vertical components (the strongest one), as represented in figure 35, but it does produce peaks in the longitudinal component ( $B_z$ ) that may impact the transverse optics. Reducing the gap down to 1 mm, reduces also the  $B_z$  peak, from 16.5 G to 10 G ; adjacent boxes are planned to be mechanically connected effectively producing a zero gap configuration.

The multi-boxes simulation also highlights the feedthrough openings effect on the suppression; this is in fact so small that it did not show up on the single box simulations nor measurements.

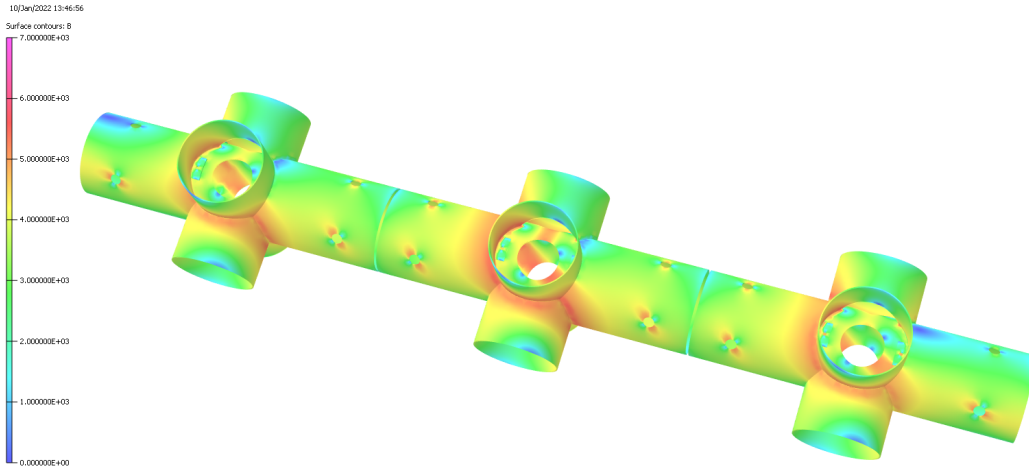


Figure 34: OPERA simulation with three adjacent shielding liners separated by a 5 mm gap. Notice that the gap is half-way between the location of the feedthrough openings (compare with figure 35).

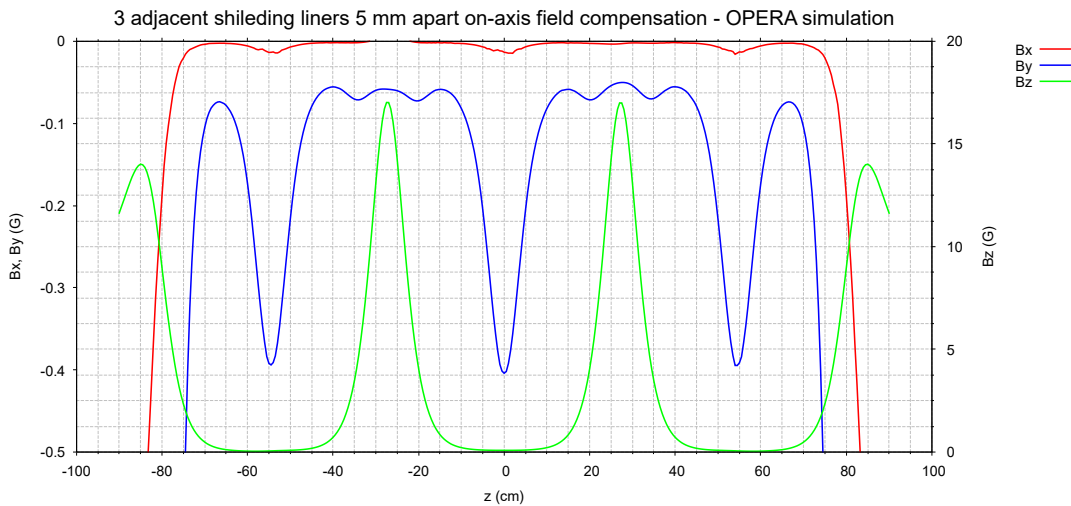


Figure 35: OPERA simulation with 3 consecutive boxes separated by a 5 mm gap. The small humps in  $B_y$  (blue curve - primary vertical axis) are due to the feedthrough ports.

Even though the in-house mock-ups perform to an acceptable level, it is expected that an improved design accompanied by a more robust fabrication (welding and re-annealing) with properly sourced material will yield a better performing shielding.

Replacement of the ISIS horizontal injection beamline TRI-DN-22-05		
Document-218327	Release No. 02	Release Date: 2022-10-25

The active compensation system consists of several pair of external coils distributed along the beamline; each Helmholtz-like pair is individually set to compensate the local stray field.

Two basic configurations, constructed according to the calculations presented in TRI-BN-20-18 [13], are shown in figure 36. The coil pair basic dimension, the vertical separation  $h$  as in TRI-BN-20-18, is chosen in order to clear the diagnostic ports, and to allow for the installation of the diagnostic devices. The single large pair (figure 36 - left) has  $h = 20$ , while the double compact pair (figure 36 - right) has  $h = 10$  (see also table 1 in [13]) These two are the simplest possible layouts, including coil geometry, which minimize complexity in term of both fabrication and controls.

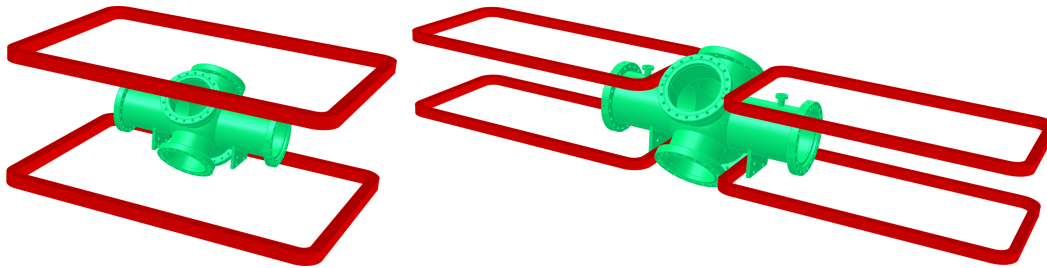


Figure 36: Possible Helmholtz-like pair configurations: single large pair (left) and double compact pair (right). Both configuration have been constructed based on the calculations in TRI-BN-20-18 [13], and allowing clearance for the diagnostic ports and devices.

The following considerations on the passive system does not take into account the fact that the coil pairs need to be clocked to compensate for the horizontal component of the stray field (here we are considering just pure vertical compensation), and that they require a support structure; both these aspects add complexity to the system.

OPERA simulations have been conducted for both coil configurations in order to see the on-axis compensation for the same background field used in the case of the passive system.

The single large coil, on its own, provides a great way to compensate for the stray field as shown in figure 37. Notice that the horizontal background component is not compensated since the coils are not clocked to generate a horizontal field.

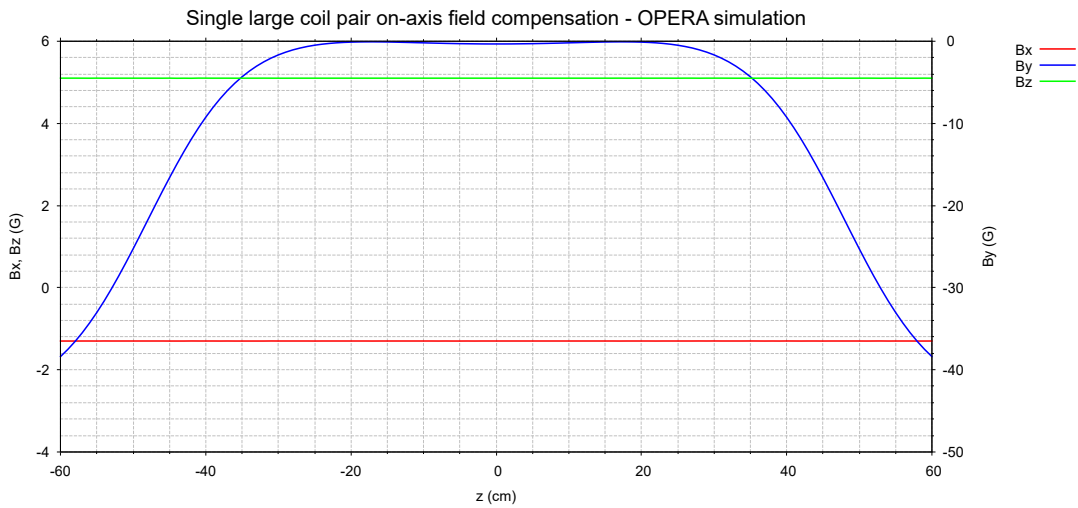


Figure 37: On-axis stray field compensation for the single large coil pair configuration (see figure 36 left side)

The double compact pairs do not perform well, as shown in figure 38, in particular at the diagnostic box location where the background field is actually augmented, as expected; this configuration requires an additional pair of coils at the diagnostic box location. As already mentioned above, this is a similar situation of the existing beamline where the limitation of positioning the soft-steel around the diagnostic boxes requires additional compensation in the form of permanent magnets.

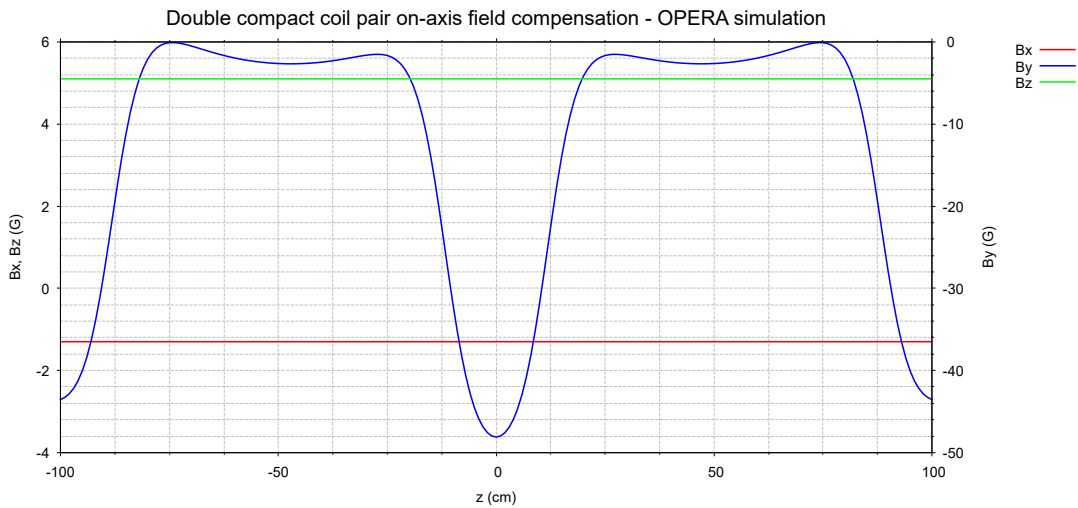


Figure 38: On-axis stray field compensation for the double compact coil pair configuration (see figure 36 left side).

Back to the single large pair, this configuration is going to be repeated in a series of adjacent pairs, as shown in figure 39.

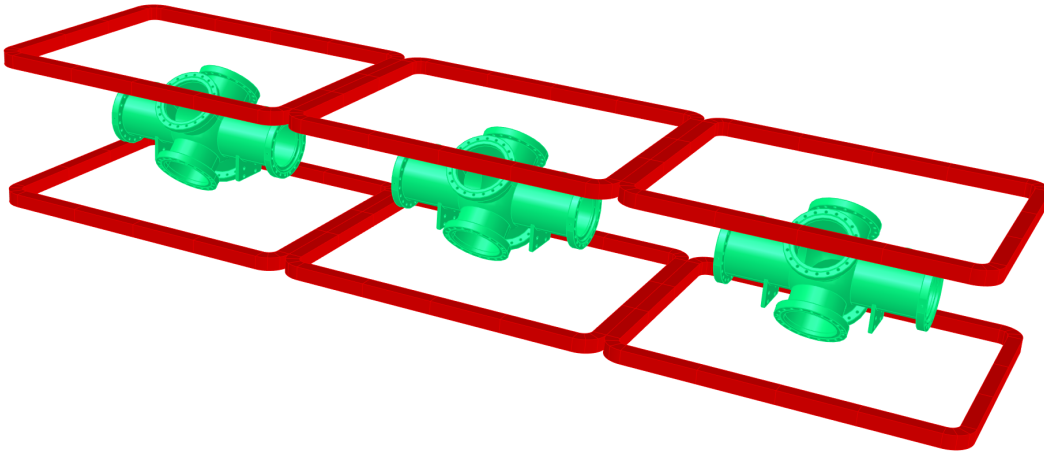


Figure 39: Three adjacent (no gap) large coil pair: to optimize the suppression (see figure 40) the central coil pair is run at  $138.5 \text{ A/cm}^2$ , while the external ones are run at  $127.5 \text{ A/cm}^2$ .

This new overall layout highlights the limitation of this configuration as well; adjacent coil pairs need to be tuned to different strengths, even for a constant background field, generating a poor compensation where the coil butt together. The on-axis compensation for this configuration is shown in figure 40.

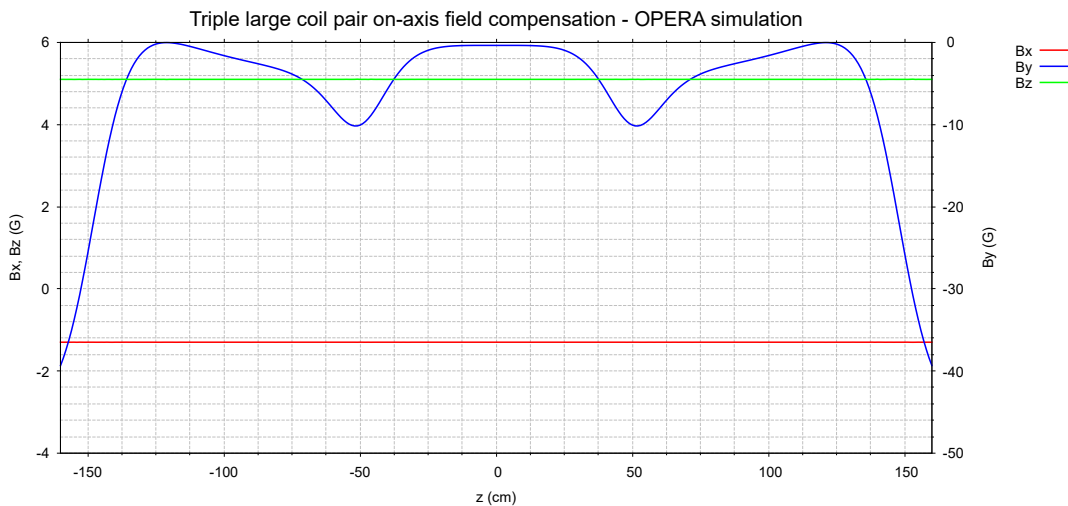


Figure 40: On-axis stray field compensation for the single lager coil configuration (see figure 36 left side).

Replacement of the ISIS horizontal injection beamline TRI-DN-22-05		
Document-218327	Release No. 02	Release Date: 2022-10-25

The main characteristic of the two compensation systems are reported in table 13. The comparison indicates that the passive system not only perform to the required level, but it is far more simple to implement with no controls and no support stand required.

One draw back of the passive system is the additional surfaces out-gassing in vacuum; this seems to be manageable as far as operating the system in the  $10^{-8}$  Torr range.

In conclusion, the selected compensation system to be implemented is the passive one.

Characteristics	$\mu$ -metal shielding	Helmutz-like coils
compensation	passive	active
power supplies required	no	yes
controls required	no	yes
vacuum load	yes	no
support structure required	no	yes
average field after suppression (G)	< 1	> 9 (compact) > 3 (large)
weight (Kg/m)	8	26 (compact) 77 (large)
cost (k\$ CAD/m)	1.4	2

Table 13: Compensation system comparison: multiple adjacent shielding liners and pair of coils are compared.

Replacement of the ISIS horizontal injection beamline TRI-DN-22-05		
Document-218327	Release No. 02	Release Date: 2022-10-25

## 7 Machine protection system

The main component of the machine protection system is the current read-back of the optical element (quadrupole, steerers and benders) bias skimmers; the skimmers, and the connected ceramic protection plates in the case of quadrupoles and steerers, are biased at 300 V. Figure 41 provides a representation of the quadrupole skimmers and ceramic protection plates.

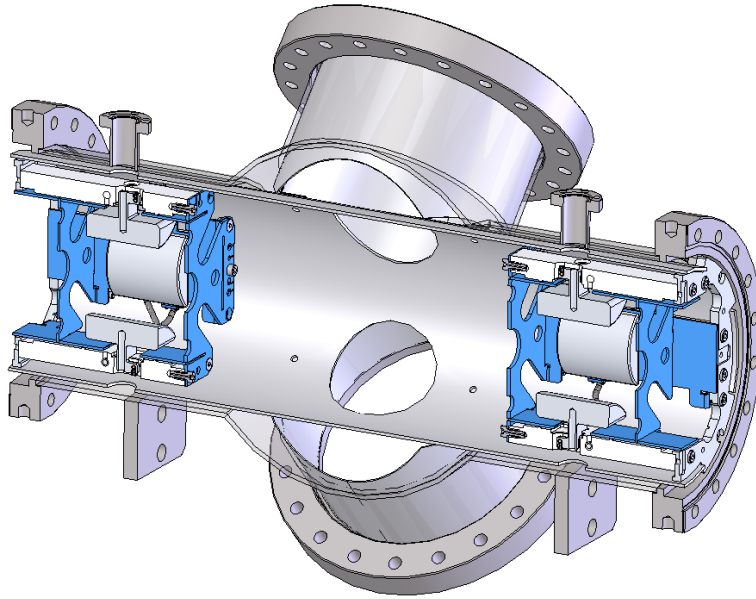


Figure 41: Quadrupole biased skimmer and ceramic protection plates (in blue); the bias voltage is 300 V to capture electrons that may be generated by the beam lost on the skimmer plates.

The bias is meant to attract the electrons which may be generated by the 300 keV  $H^-$  beam lost on the skimmer plates. This is the same protection mechanism utilized in the current injection beamline; in the new beamline though the number of skimmer is double having each quadrupole a skimmer both upstream and downstream while the current installation has only an upstream skimmer.

The intent is to read out the skimmers and ceramic protection plates as a unit for each element.

Replacement of the ISIS horizontal injection beamline TRI-DN-22-05		
Document-218327	Release No. 02	Release Date: 2022-10-25

## 8 Tolerances

The clearance of an aperture radius along the beamline should be at least 12.7 mm in order to provide a beamline acceptance of about 45  $\mu\text{m}$  or higher. Mechanical and electrical tolerances (see Table 14) for the optical elements are calculated according to the guidelines given in reference [15].

Elements	$V$ [kV]	$f$ [mm]	$x$ [mm]	$\theta$ [mrad]	$\Delta x$ [mm]	$\Delta z$ [mm]	$\Delta V$ [V]
Matching quads	2.999	288.9	4.4	8.4	0.3	4.3	4.0
Periodic quads	3.806	437.5	3.5	4.8	0.4	13.0	8.0
Low beta quads	7.642	217.9	4.2	6.8	0.2	6.5	6.0
Bender quads	3.591	463.7	3.1	5.1	0.5	11.0	10.0
45° bender	30.24/-28.76	242.6	1.9	3.9	0.2	8.0	3.8

Table 14: Mechanical and electrical tolerances of the optical elements (for  $\varepsilon = 6 \mu\text{m}$ ).  $V$  is the maximum voltage of the element (for 295 keV beam).  $f$ ,  $x$ ,  $\theta$  are focal length, beam (half-)size and beam (half-)divergence, respectively.  $\Delta x$ ,  $\Delta z$ , and  $\Delta V$  are tolerances for transverse position, longitudinal position and voltage. The roll angle of the elements should be less than 1 mrad.

Replacement of the ISIS horizontal injection beamline TRI-DN-22-05		
Document-218327	Release No. 02	Release Date: 2022-10-25

## References

- [1] R. Baartman, "TRIUMF 300 keV Vertical Injection Line", <http://lin12.triumf.ca/text/Talks/2015ECPM/ISIS.pdf>
- [2] R. Baartman, "Optics Design of the ISIS Vertical Section Replacement", TRI-DN-09-11, TRIUMF document-22849, <http://lin12.triumf.ca/design-notes/2009/TRI-DN-09-11.pdf>,
- [3] M. Marchetto, S. Saminathan, "ARIEL Front-End Desing Note", TRI-DN-11-08, TRIUMF document-41767, [http://lin12.triumf.ca/text/design\\_notes/TRI-DN-11-08\\_ARIEL\\_Front-End.pdf](http://lin12.triumf.ca/text/design_notes/TRI-DN-11-08_ARIEL_Front-End.pdf)
- [4] S. Saminathan, "Requirements for the cyclotron injection beam-line upgrade", TRIUMF document-190702, <https://documents.triumf.ca/docushare/dsweb/Get/Document-190702/Requirements%20for%20the%20Cyclotron%20injection%20beamline%20upgrade%20-%20Document%20190702.pdf>
- [5] K. Jayamanna, S. Saminathan, "Requirements for a new H- ion source for TRIUMF 500 MeV cyclotron – I2 Terminal", TRIUMF document-192303, <https://documents.triumf.ca/docushare/dsweb/Get/Document-192303/Requirements%20for%20a%20new%20H-Ion%20Source%20for%20TRIUMF%20500%20MeV%20Cyclotron%20-%2012%20Terminal%20-%20Document%20192303%20-%20Release%201.pdf>
- [6] S. Saminathan, "Beam transport for the new ion source injection terminal I2", TRIUMF document-213184, <https://documents.triumf.ca/docushare/dsweb/Get/Document-213184/NoContent5708220357140426316.txt>
- [7] R. Baartman, "ARIEL Quad Effective Lengths, Fringe Field Integrals", document-TRI-BN-19-22, TRIUMF Internal report, December 2019, [http://lin12.triumf.ca/text/design\\_notes/b2019\\_22](http://lin12.triumf.ca/text/design_notes/b2019_22)
- [8] Baartman, R A and Dutto, G and Schmor, P W, "The TRIUMF high efficiency beam bunching system", Proceedings of the Tenth International Conference on Cyclotrons and their Applications, East Lansing, Michigan, US, 1984, <https://accelconf.web.cern.ch/c84/papers/b39.pdf>
- [9] V. Zvyagintsev, *Private communication*, TRIUMF, June 2022.
- [10] A. Friedman et al., *Computational Methods in the Warp Code Framework for Kinetic Simulations of Particle Beams and Plasmas*, in IEEE

Replacement of the ISIS horizontal injection beamline TRI-DN-22-05		
Document-218327	Release No. 02	Release Date: 2022-10-25

Transactions on Plasma Science, vol. 42, no. 5, pp. 1321-1334, May 2014.

- [11] P. M. Jung, T. Planche, and R. Baartman, *Hybrid macroparticle algorithm for modeling space charge*, in Phys. Rev. Accel. Beams, vol. 25, Aug. 2022, = <https://link.aps.org/doi/10.1103/PhysRevAccelBeams.25.084602>
- [12] B. Dos Remedios, "ISIS horizontal beam line stray magnetic field mapping and compensation", TRI-BN-21-14, TRIUMF internal report, August 2021, [http://lin12.triumf.ca/text/design\\_notes/ISIS\\_Horizontal\\_Beam\\_Line\\_Stray\\_Field\\_Mapping\\_and\\_Compensation.pdf](http://lin12.triumf.ca/text/design_notes/ISIS_Horizontal_Beam_Line_Stray_Field_Mapping_and_Compensation.pdf)
- [13] R. Baartman, "Magnetic field compensation for ISIS", TRI-BN-20-18, TRIUMF internal report, December 2020, [http://lin12.triumf.ca/text/design\\_notes/Four-wire-comp.pdf](http://lin12.triumf.ca/text/design_notes/Four-wire-comp.pdf)
- [14] R. Baartman, "Magnetic field compensation for E-linac", TRI-BN-10-03, TRIUMF internal report, September 2010, [http://lin12.triumf.ca/text/design\\_notes/b2010\\_03.pdf](http://lin12.triumf.ca/text/design_notes/b2010_03.pdf)
- [15] R. Baartman, "Tolerances in the LEBT Optics", TRI-DN-97-11, TRIUMF internal report, November 1996, [http://lin12.triumf.ca/text/design\\_notes/t1997\\_11/optics\\_tol.pdf](http://lin12.triumf.ca/text/design_notes/t1997_11/optics_tol.pdf)